Applications of Remote Sensing to Agribusiness

Jack F. Paris, Ph.D.
Director
Spatial Information, Visualization & Analysis Resources Center
California State University Monterey Bay
100 Campus Center
Seaside, California 93955-8001 USA
Telephone 408-582-4221; FAX 408-582-3073
Jack_Paris@Monterey.edu

Abstract

Agriculture has used remote sensing (RS) for many decades. Starting in the 1930s with panchromatic aerial photography for farmland and soil surveying, RS applications to agriculture expanded greatly with the invention of ordinary color and color infrared (CIR) films.

The Landsat program brought digital optical RS to some sectors of agriculture on a global scale. Information extraction based on changes over time became possible with the frequent and regular revisit nature of spacecraft-based RS like Landsat. In the AgRISTARS Program, NASA used Landsat to explore multispectral (MS) RS for crop identification and yield assessment for major global crops. The importance of temporal signatures became obvious through this effort. The Thematic Mapper (Landsats 4-5 and soon, Landsat 7's ETM+) expanded global MS RS to include middle infrared (MIR) and thermal infrared (TIR) bands.

Aircraft-based MS RS systems have continued to be the primary sensors for agriculture. Digital color, CIR & TIR cameras now allow quick delivery of RS images and related information products to agribusiness with high resolution on a weekly basis.

In the near future, great advances will likely occur. MS RS at 4-m resolution will soon be available from space. Hyperspectral RS will be available in some regions. Spacecraft-based multiparameter SAR will cover areas that have historically been denied to optical RS due to cloudiness. These new capabilities will bear on many agribusiness interests heretofore not well served including precision farming, crop risk insurance, and ag-related financial institutions.

Introduction

Converging Technologies and Applications is a very appropriate conference theme, especially for agricultural applications. *Agriculture* was, of course, one of the first human-invented technologies. Agriculture has freed much of humankind from the rigors of the hunter-gatherer way of life. And agriculture made possible the *Industrial Revolution*, which, in turn, greatly improved the efficiency of agriculture enterprises so that now a few are able to feed many. Today, we are firmly in the *Information Age and the Space Age*. Agriculture is still in the forefront of technological innovations taking place in the collection and use of information.

My purpose here is to look toward the next decade of exciting advances likely to take place in remote sensing (RS) applications for agriculture. Note that I assume, in this paper, that RS includes both photographic and non-photogrammetric systems. I will start by reviewing some of the past developments in RS as they relate to agriculture. These provide a historical perspective of events leading to the state of RS technology today for agriculture. In addition to RS, many other related geospatial technologies are involved – image processing (IP), geographic information systems (GIS), global positioning systems (GPS), spatial analysis (SA), and visualization technologies (VIS). As it should be, this Conference is not just about RS and photogrammetry. Rather, it is about the whole alphabet soup of related geospatial technologies

including RS, photogrammetry, IP, GIS, GPS, SA, and VIS. I hope that these technologies, working together, will spell relief for many of the nagging problems that confront humankind as we attempt to balance ecology and economics. I am confident that they do.

The multiple geotechnologies are now converging and taking shape as information systems designed for real-world applications. A glance at the wide-ranging content of this Conference shows how heretofore separate technologies have converged or are converging. Global ecological applications now use just about every possible RS approach – high-resolution visible imagers, shortwave optical MS systems, longwave optical thermal infrared mappers, passive microwave devices, and active microwave (radar) systems. Digital (softcopy) photogrammetry has essentially replaced strictly film-based (hardcopy) photogrammetry. Digital-imagery and derived raster-based information are members of the GIS family. GIS used to include only vector and CAD elements and their attributes. RS data users now commonly employ image processing, spectral analysis, and spatial analysis tools in a GIS framework. Data intensive RS technologies such as radar polarimetry, radar interferometry, and hyperspectral systems may become operational as advances occur in data storage and retrieval technologies and in computer processing and communication systems.

Agriculture is also benefiting from these and other converging technologies (Runyon, 1994). More and more growers, vendors, crop consultants, pest control advisors, irrigation specialists, and agronomists are using GPS technology to record precisely the spatial locations of field-collected information. GPS is used to navigate to areas of concern perhaps as indicated by georeferenced RS data. GPS and variable rate technology (VRT), driven by georeferenced RS data and/or georeferenced data from yield monitoring technology (YMT), allows precision applications of chemicals and water within a managed field. At harvest time, yields are being mapped for inclusion in a GIS. Off-season soil amendments and irrigation system designs are based more and more on data obtained from geospatial technology. Aerial survey firms are offering mapping and monitoring services to agribusiness in more and more regions. In a few years, we will see significant advances in these kinds of services on a global scale with reliable information provided on a weekly basis, within a day of acquisition, and in end-user friendly formats compatible with affordable software packages running on powerful desktop computer/software systems.

Before I start the balance of this paper, let me make it clear that I am not trying to provide a comprehensive review of all RS applications for all of agriculture. This task is too great for one person to accomplish and is too broad to be covered in one keynote address. Rather, I want to give a personal view of the development of applications of RS and related technologies for agriculture. My RS-for-ag career began in July 1972 with the launch of the Earth Resources Technology Satellite (later dubbed *Landsat 1*). It continues today with the current proliferation of complex RS systems on a bewildering array of spacecraft and aircraft. I need to point out that I came into this remarkable 26-year period of time from the perspective of a physicist, a mathematician, a weather forecaster, and a hydrometeorologist. Recall that the first practical applications of RS were for meteorology and oceanography. This started with surface-based weather radar in the 1940s and continued into the 1960s and to the present day with satellite-based imaging systems such as TIROS, AVHRR, and GOES. My previous experiences were helpful -- photo interpretation (including photos of the earth from Apollo) and with photogrammetry (via civil engineering) as well as with cartography (geography) and with radiative transfer of electromagnetic radiation (mostly microwave) from ocean and land surfaces through cloudy and clear atmospheres. Nevertheless, July 1, 1992, was a significant day for me. On that day, the Division Chief, Dr. Robert MacDonald, at the NASA Lyndon B. Johnson Space Center had the gall to divert me from my comfortable academic studies of passive microwave RS. Bob asked me to lead one of the teams investigating multispectral (MS) data from ERTS (Landsat 1). This experience launched me into the world of RS applications for land features including those of interest to agriculture and agribusiness.

This first experience with MS RS digital data and image processing algorithms for a coast land area near Houston, Texas, led to a lifetime of work on soil moisture estimation, crop identification, and crop condition assessment with a wide variety of crops and soils throughout the US. Eventually, I changed from doing basic research at places like NASA JSC and the Jet Propulsion Laboratory and turned more to applications research in universities and in private enterprise. Since 1989, I have been involved in the development of applications of multisensor (MS and radar) RS mostly for the commercial systems that exist today or that will exist in the near future for agriculture.

Natural RS, IP, and GIS

Humans are, in fact, quite familiar with RS. Natural human *vision* has been and still is the most significant form of RS. Beyond vision, humans can *feel* thermal infrared (TIR) with their hands and can use *hearing* for RS by sound. *Smelling* might also be considered to be RS. In addition, humans possess a wonderful *image processing* (IP) capability. This involves both the eyes and the brain. Most of us possess an excellent stereo vision system; I don't. Humans preprocess visual information from an irregular array of visible light detectors (the rod cells in the retina that respond mostly to green light). Mixed in with the rod cells are cone cells that add color properties (hue and saturation) to human vision. Then, humans perform parallel processing of these disparate spatial data via a neural network (the brain). All of this happens in real time including the seamless mosaicking of patches of images acquired as the eye scans around from object to object in our vicinity. Then, we put all of this complex spatial information into an on-going dynamic GIS-like model of our external world. This is a 4D system with the element of changes over time enhancing the 3D spatial information that we directly perceive. Again, this is all done in real time.

In my option, there are 6 fundamental human weaknesses in our natural RS, IP, and GIS system:

1. We do not have an objective view of spatial information. Things close to us are more important than things distant from us. We cannot easily see the big picture.

2. We tend to forget details about previously seen spatial information. Old information lacks clarity and detail. We have trouble seeing trends or changes over time.

3. We do not know our absolute location except in relationship to known landmarks.

4. We cannot see how things look outside of the visible spectrum (400 to 700 nanometers in wavelength). Important information exists in the UV, NIR, MIR, TIR, and microwave.

5. We cannot easily perceive information at different scales. Both the microscopic and the macroscopic are not perceived naturally. We need microscopes and macroscopes (GIS).

6. We cannot easily integrate information about objects not within our immediate view. Hence, the saying, "out of sight, out of mind."

To overcome these natural limitations, we have invented geospatial technologies – first mapping (drawings, cartography, surveying), then writing (database recording), then photography (image recording), then RS (non-photographic imaging), then IP (information extraction, enhancement), then GIS (computer-based mapping and spatial analysis), and then GPS (easier surveying).

Agriculturists, being human, also possess these natural RS, IP, and GIS abilities and carry these into their fields, farms, and ranches. I find it interesting that when an agriculturist first encounters an RS technologist (like me), he or she is often skeptical about RS, IP, GIS, GPS, etc. After all, agriculturists have walked the fields, have used eyes and brains while doing so, and therefore believe that they know all there is to know about the subject fields. What an agriculturist fails to realize is that (1) the perspective of a field from within a field is not very good, (2) human memory

is poor, (3) there is more than meets the eye, and (4) things at other scales are not seen. A *downward-looking, recorded* view from a lofty place goes far towards addressing these human failings even if the image acquired looks like what humans see (i.e., is like ordinary visible color). The down-looking perspective is superior even if the view lacks color! If the aerial view goes beyond human vision into the unseen – shortwave infrared, longwave infrared, and microwave – then down-looking RS data are even more useful. It is important, I think, that an RS practitioner eventually make *invisible* RS data (better yet information) visible in forms that can be comprehended by humans as spatial images in color that change over time (animate) and that appear to be three dimensional.

Now it is time to consider technological RS, rather than natural RS, as it has been used for agriculture.

Panchromatic Airphotos: The First Use of RS for Agriculture

Photography was invented in the mid 1800s. These earliest photos produced only monochrome (single color or grayscale) images. In addition, early photos were sensitive to only ultraviolet radiation [UV, 300-400 nanometers (nm)] and to blue light (BL, 400-500 nm).

Truly panchromatic photography (300-700 nm) was invented in the late 1920s. *Panchromatic* (*pan, for short*) means "across all colors." Thus, pan photos record (as a grayscale image) reflected light for all wavelengths in the human perceived visible light region (400-700 nm). Pan photos also retain their sensitivity to the UV.

Aerial pan photography with accurate "metric" frame cameras was first used for agriculture by the Soil Conservation Service to carry out the soil mapping mandates of the Soil Conservation Act of 1935. Aircraft-based, vertical, metric *pan photos* greatly aided soil surveying and field mapping. Soil attributes were acquired by intensive ground-based sampling. Eventually, soil polygonal lines were drawn over rectified aerial pan photos. This predated the use of polygons in modern GIS.

Monospectral RS

We often hear these days about multispectral RS. But, in the beginning, there was only *monospectral* RS. A aerial pan photo is an example of a monospectral RS approach where the resulting grayscale tone of the image is a record of the brightness of reflected solar radiation in a single, albeit wide band of reflected solar electromagnetic radiation (EMR). Pan photo film responds to a wide range of wavelengths including UV, BL, green light (GL, 500-600 nm), and red light (RL, 600-700 nm). In the early 1940s, monospectral film sensitivities were extended into the near infrared (NIR) out to about 900 nm. Pan IR film covers UV and visible light as well as NIR radiation. It had immediate usefulness as a camouflage detection film in World War II. Herbaceous vegetation is bright in the NIR, but artificial (camouflage) vegetation is not.

With an UV & BL minus filter, common pan photos cover primarily the GL and RL parts of the visible EMR. Blocking UV & BL exposures improves the quality of the resulting pan photo image by reducing the degrading effects of light scattering in the atmosphere between the aerial observer and the ground. Filtering visible light from pan IR film also produces desirable effects.

The great advantage of modern pan photography is that it has superior spatial resolution compared to color film or to MS RS systems (given the same focal length). Well taken pan photos can be used by trained and even by amateur photo interpreters to identify land features by virtue of their size, shape, pattern, texture, and tone. Shadows, temporal patterns, and context are also useful. With overlapping metric pan photography and stereo analysis techniques, precise orthographic photogrammetry is possible. Detailed pan photos now exist for much of the US. These may be corrected for distortions introduced by lenses, by camera tilting.

Stereo pan photos allow one to deal with distortions caused by terrain (i.e., with relief displacement). The digital orthophoto quad (DOQ) is widely available and is used for many human endeavors including agriculture (for mapping of field, farm, and ranch boundaries). A DOQ is, of course, based on the spectral properties of pan photos with UV & BL minus filters. For agricultural mapping and monitoring, a problem with existing DOQs is that they often are many years old. The other problem is that they respond to only one spectral band (at a time), i.e., they are monospectral. For some soil and for most plant characterizations by aerial photography, multispectral RS is highly desirable.

Nevertheless, high spatial resolution DOQs ranging today down to 0.1 m picture elements (pixels) are truly impressive sources of information useful for all kinds of mapping including mapping agricultural features. In the US, the government has abandoned its historic role in mapping agricultural crop and field boundaries. This responsibility now falls on private industry, e.g., the crop risk insurance carriers. This is a business opportunity for RS and derived information product vendors.

Some air photo vendors are using pan photo film with a narrow spectral filter to record the brightness of a scene in a particular part of the EMR spectrum. For example, one might use a red-light (RL) pass filter to record the chlorophyll-sensitive part of the visible spectrum near 660 nm. This approach takes advantage of the superior spatial resolution characteristics of monospectral films with its relatively low cost. However, there are several disadvantages in this kind of monospectral approach. One relates to the non-linear way that pan photo film responds to light exposure. The well-known characteristic curve for monospectral film is a plot of film density (for negative transparencies) versus the logarithm of exposure. Film density is related to the logarithm of film's transmittance. Exposure, for a given aperture, shutter speed, and focal length, depends on the brightness of light being reflected from the scene. Thus, scene reflectance has a non-linear (log-log) relationship to transmittance of the film (or to the brightness of the image being viewed or measured). This non-linear relationship between image brightness and scene reflectance makes radiometric calibration difficult. In many non-photographic RS devices, e.g., Landsat, the relationship between image brightness and scene reflectance is linear. Another disadvantage of using film is the relatively long period of time that it takes to produce an image. The film must be developed and perhaps enlarged before it can be interpreted. Long processing times can be detrimental to some agricultural applications.

Nevertheless, some vendors are using pan photos taken at regular intervals over a growing season to map soil properties and to track changes in crop conditions. I will return to this idea later after some additional background into information extraction from MS RS data. Next, I want to provide a more physical basis for RS as related to the brightness of EMR sources, the characteristics of the intervening atmosphere, the reflectance of the land surface, and the effects of source and sensor geometry.

A Physical Basis for Shortwave Optical RS

EMR brightness in a band of wavelengths is known technically as *band radiance*, L (in *Watts per square meter per steradian of solid angle*, $W\ m^{-2}\ sr^{-1}$). Since one or more bands of wavelengths are always involved in RS, I will drop the modifier term, *band*, for the rest of the discussion.

The upwelling brightness of the atmospheric path between an aerial platform and the ground is characterized by the *path radiance*, L_p. Reflectance of downwelling solar radiation (directly from the sun and indirectly from the sky) by the scene also produces upwelling *scene radiance*, L_s.

It is useful for some of the discussion that follows in this paper to formulate a mathematical model that relates the brightness, V, of an image to the reflectance, R, of the surface. In modern digital RS data processing, V is often an 8-bit unsigned integer value in an image raster. If so, V ranges

between 0 and 255. However, due to the existence of path radiance over the whole scene, raster images usually do not take on values near 0. This is an important and often overlooked characteristic of image data by those who would use standard information extraction techniques on digital image data (e.g., the production of a normalized difference vegetation index raster). I have more to say about this problem later. Right now, we need to continue with the model.

RS starts often with the irradiance of the sun, E_s (in $W\ m^{-2}$). For shortwave optical RS, the sun is the source of the radiant energy that a RS system detects and maps into an image. Note that the solid angle size of the sun and its radiance are included in E_s. Assume that E_s represents a bundle of EMR photons that are travelling toward the surface along a path denoted by a zenith angle of incidence, θ_s (in *degrees*). Due to scattering and absorption by gases and aerosols in the atmosphere, the apparent irradiance of the sun decreases along the sun-to-ground path. This reduction in E_s is characterized by a transmissivity, t_1, which has a value between 0 and 1. E_s is also reduced by a factor of the cosine of θ_s. Thus, the apparent irradiance of the sun at the surface is equal to $E_s\ t_1\ \cos\theta_s$. The reflectance of the surface, R (a fraction, but often expressed as a percentage), controls how much downwelling irradiance is scattered upward (perhaps toward an RS device). If the surface reflectance is diffuse (i.e., goes equally in all directions), the radiance of the upwelling EMR, L_s, caused by the reflecting surface is further reduced by the factor, $1/\pi$. It should be noted here that remotely-sensed information about the surface and its material nature is contained in R.

As the upwelling band radiance travels back through the atmosphere, it is attenuated again by scattering and absorption by atmospheric gases and aerosols. This reduction is parametized by another transmissivity, t_2 (which ranges between 0 and 1). After passing through the portion of the atmosphere between the surface and the aerial RS device, the scene radiance passes into the RS device and is recorded by various means. Path radiance (from the atmosphere only below the sensor) also enters the sensor to be recorded. The RS system sees these two sources of radiance – path radiance and scene radiance – as one additive stream of radiant energy (total radiance, L). The result is recorded as apparent image brightness, V. V is related to L by a factor, G, which includes the gain of the sensor as well as considerations such as the size of the field of view of the detector and the time interval over which the band radiance is recorded.

Putting all of this together, we have a simple model, Eq. (1), which predicts V as a function of R and other parameters, as follows:

$$V = G\ [(E_s\ t_1\ \cos\theta_s\ R\ t_2) / \pi + L_p] \qquad (1)$$

In film and for CCDs (charge coupled devices), G is not a constant. Rather, G varies with the total radiance or exposure (as given by the non-linear characteristic curve for the film or CCD detector used). For other RS systems (such as Landsat, SPOT, and the Indian Remote Sensing Satellite), G is a constant parameter for a given band and sensor regardless of scene brightness. Of course, G varies from band to band and may change over time. In aircraft systems, G also changes with changes in the aperture and shutter speed of the camera (which is often changed during a flight by the camera operator on board the aircraft). In a spacecraft system, G changes slowly over the lifetime of the system. In general, humans do not mess with aperture and shutter speeds for spacecraft systems. In this context, beware of automatic gain systems. They may be great for producing proper exposures, but they create havoc in attempts to perform radiometric calibration.

Many other kinds of interactions can be brought into the model. One example is the inclusion of the adjacency effects of dark objects surrounded by light objects and vice versa. In addition, some use full-blown radiative transfer models to model the relationship between V and R. R, itself, may be represented by a bi-directional reflectance factor function that depends on physical and geometric terms. In such complicated models, it is easy to lose sight of the important variables in the relationship between V and R.

While the foregoing equations give a quantitative, mathematical relationship between image brightness, V, and surface reflectance, R, this relationship requires a great deal of knowledge about the atmosphere. Generally, the state of the intervening atmosphere is unknown at the time that RS data are acquired. Innovative approaches exist to use multi-angle RS data or to use multispectral RS data to independently estimate atmospheric and surface characteristics. Even without these again more complex approaches, Eq. (1) is neither practical nor solvable in most RS situations. Nevertheless, this simple model serves for an empirical approach to calibration.

If the look down angle is small (essentially zero), if the atmosphere is horizontally homogeneous over the extent of the imaged area, *and* if the gain, G, of the RS is constant, then the model reduces to a simple, useable form, namely,

$$V = V_p + R / m \qquad (2)$$

Thus,

$$R = (V - V_p)\, m \qquad (3)$$

where $\mathbf{V_p}$ is the image brightness value that corresponds to path radiance (assumed to be constant over the extent of the imaged area) and **m** is a multiplier that transforms image brightness values to scene reflectance. Note that $\mathbf{V_p}$ and **m** are calibration constants that allow one to calculate R from a given V via Eq. (3).

The foregoing ideal situation can be invalid. If the look down angle is large, *or* if the atmosphere varies over the extent of the imaged area, *or* if the sensor response (G) of the RS is non-linear, then no simple linear relationship exists between V and R. In fact, a higher value of V does not necessarily imply that a higher value of R exists; the path radiance may simply be much higher in one place compared to another.

Look down angle effects can be very severe. If one looks directly away from the sun (toward the shadow of the aircraft), one sees that V (and R) appear to be much brighter for the same surface object than what is observed directly under the aircraft. This is called the hot spot effect. If one looks back, in angle, towards the sun, one sees that V (and R) appears to be much darker. This is due to the effects of small shadows (e.g., leaf on leaf) being visible or not as look down angles change. Camera geometry can also lead to image darkening toward the corners of the image. These look down effects on image brightness (and on implied values of R) are about the same for all bands. Thus, ratio indices among bands tend to reduce the seriousness of look down effects. Look down effects can also be minimized by making sure that the hot spot exists outside of the extent of the imaged area (i.e., when the irradiance direction is far from being overhead). Thus, the time of day for image data acquisition is important, especially for summer months in low latitudes when the sun may be overhead at or near the local solar noon.

If Eqs. (2) and (3) are valid, then the two calibration parameters, $\mathbf{V_p}$ and **m**, can be determined by observing the image brightness of black (R = 0) or shadowed ($E_s = 0$) objects. Then, by making another observation of image brightness, V_b, for a level (flat) object of known reflectance, R_b., one can estimate **m**. Note that the object of known reflectance needs to be moderately bright (reflective). Be careful, however, to avoid extremely bright objects that have saturated the sensor (i.e., that have driven V to the top of the scale, 255). Explicitly,

$$m = R_b / (V_b - V_p) \qquad (4)$$

Any given spectral band of the Landsat Thematic Mapper (TM) is a linear monospectral RS system. By linear, I mean that the values of $\mathbf{V_p}$ and **m** in Eq. (6) are constant over the extent of the imaged area.

Let's now turn our attention to a specific set of RS data. This set includes both multispectral shortwave and longwave RS data (a collection of several monospectral RS data) as well as

multifrequency, multipolarization synthetic aperture radar (SAR) data taken in the same 16-day period of time over an agricultural area.

RS Image Data for Irrigated Cropland in the San Joaquin Valley

To illustrate the way that I approach RS data for agricultural applications, I have selected a set of TM data (April 5, 1994, and April 21, 1994) as well as a set of synthetic aperture radar (SAR) data (April 15, 1994). I collected (e.g., imported), manipulated (e.g., geocoded, resampled, and enhanced), managed, analyzed (e.g., information extraction), and presented these data by using TNTmips by MicroImages, Inc., Lincoln, Nebraska, USA.

Figure 1. A red light image (TM Band 3, 630-690 nm) of a portion of southwestern Fresno County, California, USA, acquired on April 5, 1994. The green square shows a square mile section of land. The latitude/longitude map coordinates of the section's center appear in the lower right corner (North American Datum 1927 for the Western US.).

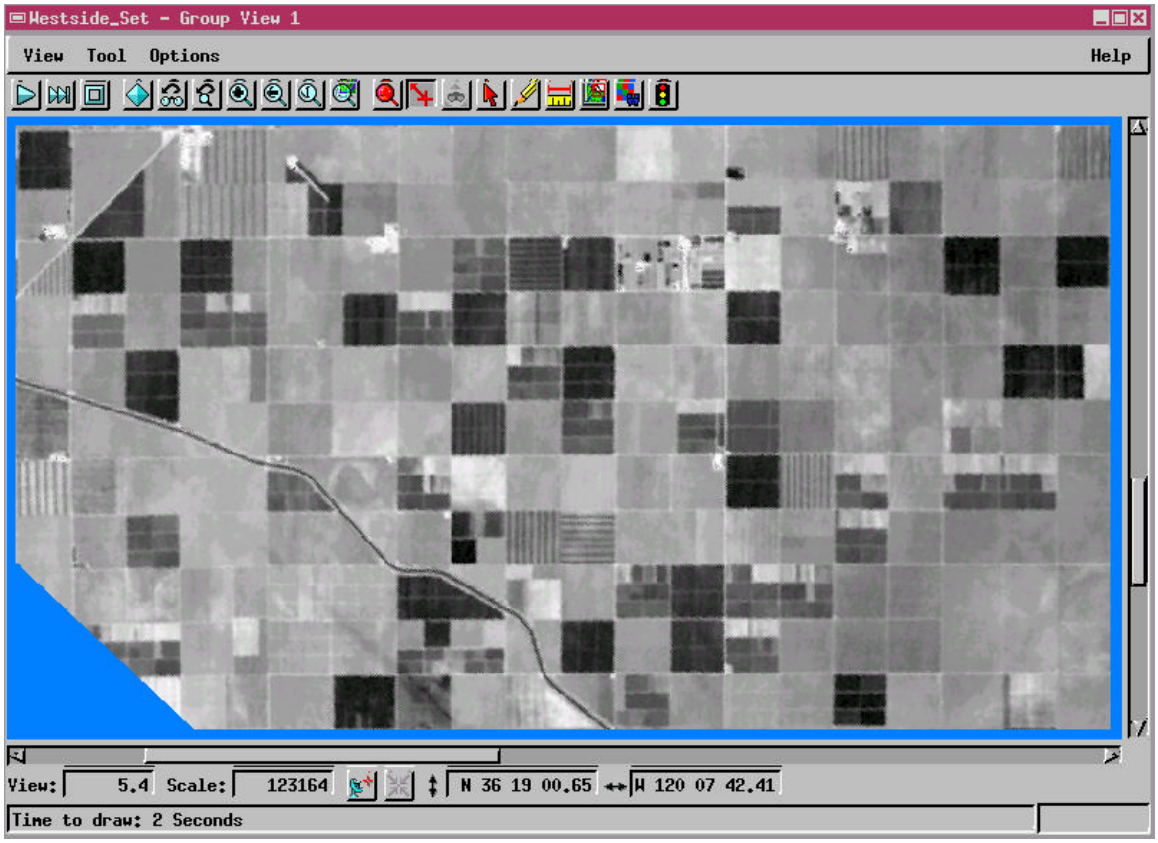

Other RS data are on hand for this area for the same month, namely (1) more TM bands for April 5, 1994, a set of TM bands for April 21, 1994, and (3) a set of Shuttle Imaging Radar (SIR-C) image data for on April 15, 1994. These three concurrent image data sets and concurrent crop information from the Westlands Irrigation District form an interesting multisensor data set to illustrate some of the points being made in this paper. The original instantaneous field of view (IFOV) for the TM data was 30-m by 30-m. The "IFOV" for the SIR-C data was 22-m by 27-m.

Site Description

The California Aqueduct, the major backbone of the Central Valley Water Project, travels from the west edge of the site to the south edge of the site. This is a concrete waterway that travels from northwest to southeast down the western edge of the San Joaquin Valley. It provides fresh water to the extensive irrigation systems in the Westlands Irrigation District that serves this region. Most of the agricultural fields are quarter sections (160 acres) with section and half-section roads at the edges of the fields. Most of these roads are dirt roads. Many of the quarter sections are divided into smaller units. A major paved two-lane highway cuts across the northwest corner of the site with a southwest to northeast orientation.

Major known crops are indicated by various colored polygons in Figure 2.

Figure 2. Selected crops for the area shown in Figure 1. Background is the TM Band 3 image.

Some (■) crops are permanent crops – almond orchards, apple orchards, and a vineyard. Lettuce fields (■) are being harvested, small plot by small plot by hand. Garlic (■) is in mid season. Sugarbeets (■) are in mid season. A few onion fields (white) exist. One cabbage (■) field is ready for harvest. The range of crops in this region serve well to illustrate different RS approaches including monospectral RS, multispectral RS, thermal infrared RS, radar RS, and multisensor RS. The 16-day time span of these data also allows me to illustrate possible uses of changes over time as a way to extract information.

Bare fields cover about half of the site. The predominant top soil is Panoche clay loam derived from the California Coastal Range (which lies to the southwest and which is a mostly sedimentary rock area with little rain). The San Andreas Fault runs through this range. Many of the bare fields were being prepared for planting summer or fall crops such as cotton, tomatoes, and cantaloupe.

Some fallow fields are present. The University of California West Side Field Station is near the top just east of the center. It has small experimental fields of crops found other places in the larger region.

Preparatory Image & GIS Processing

Geocoding. First, I added a set of georeferencing control points to the TM and SIR-C image data sets. I used a scanned and georeferenced map (1:100,000 scale) as a reference for these georeferencing operations. Then, I resampled each set to match each other with 20-m cells and north at the top. Since the SIR-C data were obtained over a narrow range of angles, standard warping models worked well. In other cases, where airborne SAR data are used, then I would use a special processing script that I developed using TNTmips' Spatial Manipulation Language (SML) instead of standard warping models to change from slant range to ground range projection.

Interior Field Polygons. I used the TNTmips Object Editor to create the GIS vector polygon overlays in Figure 2. First, I created a set of GIS vector lines that ran down all visible section and field roads. Then, I used vector GIS buffering process in TNTmips to create polygons inside of the road polygons at a specified distance (50 m, in this case). Buffering produced island polygons completely inside a given field so that only crops and soil exist within and on the boundary of these (i.e., no road or field boundaries). Polygons of known crop type were attributed accordingly (records of an internal relational database table set attached to associated polygons). I used a query to show major classes of crops as different colors (as shown in Figure 2). Some fields (not shown) had no crop identification. Other fields (also not shown) were bare in April 1994 (e.g., tomatoes, cotton, and cantaloupe).

Univariate Statistics. I used TNTmips' histogram tools to investigate the distribution statistics of the brightness values in the TM Band 3 image raster. The results are shown, in two ways, below in Figure 3. The user can toggle between these two ways in the TNTmips package.

Figure 3. TNTmips Histogram Display tool for TM Band 3, April 5, 1994.

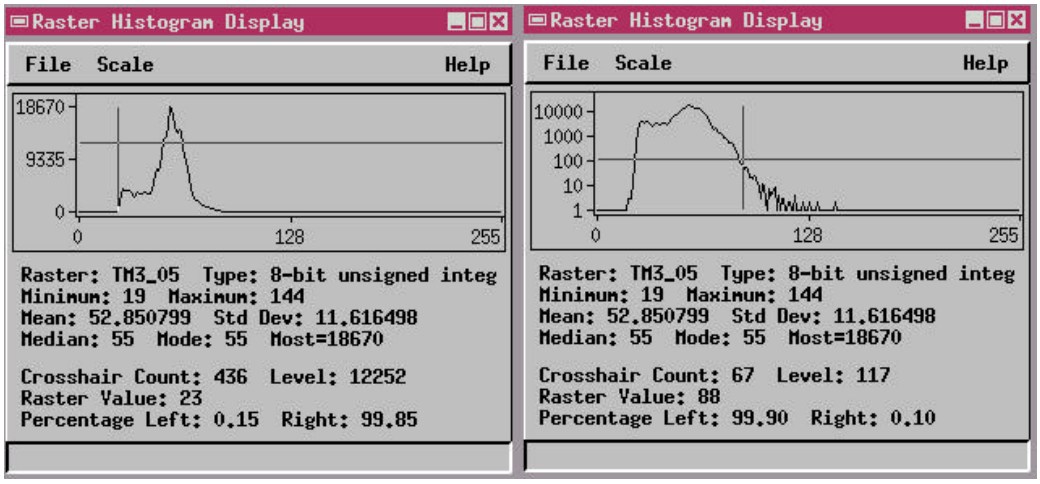

One can (and should) start the process of calibration and understanding by studying these histograms. Note, for example, that the *shape* of the histogram indicates that two basic classes of materials exist in this scene as mixtures with some relatively pure pixels in the mix. The dominant material class is bare soil (the brighter of the two). The other material class is green vegetation and open water (the darker of the two). In analyzing reflective RS data, you should focus you attention of what is dark rather than on what is bright. Darkness is due to the presence of some material (in the affected pixels) that is absorbing the EMR in the subject wavelength

band. In the case of this scene, it is the chlorophyll in the leaves and the water in the soil or in the open water areas that are absorbing.

More than likely, one would use primarily the spatial information clues in this scene (shapes of fields, sizes of areas, patterns of irrigation, texture, and context) to identify features on this landscape. This is indeed how I identified field boundaries that led to interior field polygons (as shown in Figure 2). In addition to field boundary features, one can identify fields being irrigated and fields have rows (i.e., row crops).

Nevertheless, the spectral (grayscale) characteristics of these data contain information about each field (albeit, not terribly definitive). Therefore, I want to turn your attention to the need to calibrate the grayscale brightness, V, of this scene into surface reflectance, R. This requires, according to Eq. (3), two parameters, $\mathbf{V_p}$ and **m**. Note also that the **minimum value** of TM Band 3 is **19**. Thus, *19* is a good candidate for the path-radiance equivalent raster value, $\mathbf{V_p}$, for TM Band 3. Recall that *path radiance* is the scene brightness for a black (zero reflectance) object in the scene. The maximum value of TM Band 3 is 144; however, there is no way of easily knowing what reflectance, R, this image-brightness value represents. The crosshairs in the histogram displays are set to approximately 0.1 percentile and 99.9 percentile – a range from 23 to 88. This range is a useful range for enhancing the appearance of the displayed image by using a contrast lookup table. The exponential (power law) model is useful for image display enhancement purposes. I like to use the 0.1 and 99.9 percentile points in the image brightness value histogram to be represented by the full range of displayed brightness. I also like to "bend" the look up curve by using a power exponent value of 0m7.

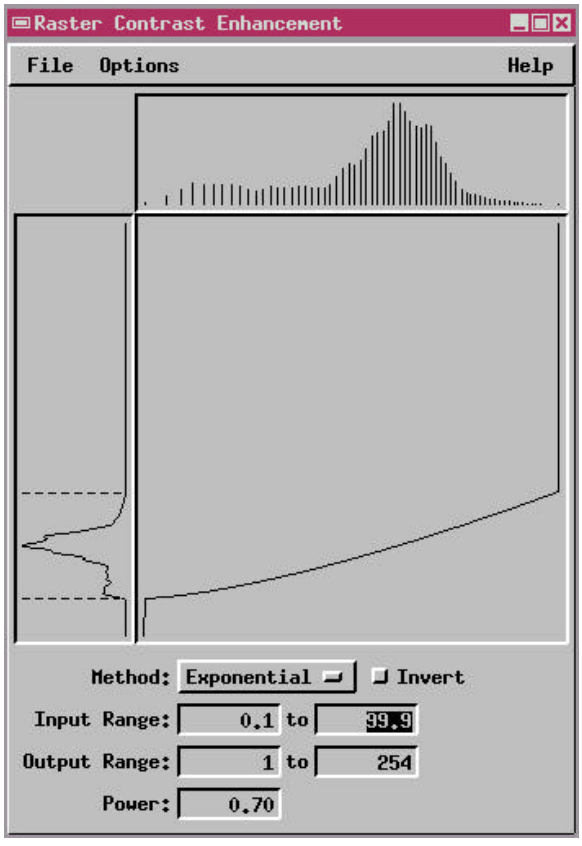

Figure 4. The TNTmips Raster Contrast Enhancement tool for TM Band 3 raster.

The vertical scale shows the distribution of the input raster data from 0 to 255. The histogram for these input data is plotted along the y-axis. It is similar to the histogram in Figure 3, but turned 90 degrees counterclockwise.

The horizontal scale shows the distribution of displayed brightness from 0 to 255. A histogram of the enhanced values thus appears at the top of the Raster Contrast Enhancement control box. Values of the lookup table used to produce displayed brightness from input raster values. A plot of the lookup table exists in the lower right hard (large) portion of the tool.

Note that I have used an Output Range from 1 to 254, rather than from 0 to 255. I like to reserve 0 and 255 in a raster for special uses (e.g., as transparent null values).

Comments on the Uses of Monospectral RS Data

It is clear from this example that crop identification is not likely to be successful if one only has one band of RS imagery, e.g., the red light ban image in Figures 1 and 2. The same would be true for any other single RS band. Anyone who has worked much with monospectral optical RS data would agree with this general statement. Nevertheless, a great deal of hype exists for high-spectral, monospectral RS data. For example, as already noted, aerial pan photos of extremely high spatial resolution are available for many regions. These often use image pixels much smaller than one meter. Very soon, one-meter pan imagery will be available from spacecraft in long-term orbit around the earth. The first example of this will likely occur this year. This would be the pan image data from systems like Space Imaging EOSAT and OrbImage 3. I do not doubt that such one-meter pan data will be quite useful. But, these will not allow for the extraction of some desired kinds of information for agriculture – especially for crop identification leaf-pigment related indicators. The same holds true for existing spaceborne pan systems such as SPOT Image and the Indian Remote Sensing Satellite (IRS) with 10-m and 5-m pan bands.

There is another class of monospectral RS image data that will be equally limited and equally successful relative to the pan image example already presented. This is the case of monospectral radar (SAR). Today, several monospectral SAR RS systems are operational. These do not produce one-meter data, but such SAR data are coming soon. There is a debate in the USA about whether monospectral SAR will be one meter or a few meters. It is interesting to me to read the hype that accompanies some monospectral SAR systems – disease detection, yield monitoring, crop identification. It seems to me that such specific kinds of information are not extractable in a consistent way from monospectral RS data (regardless of the RS region involved).

Let me now introduce a monospectral SAR image (Figure 5, next page) from the already mentioned SIR-C data set taken on April 15, 1994. This image is similar to that acquired by RADARSAT and the ERS-1 SAR. C-band has a wavelength of about 6-cm.

Figure 5. C-Band VV image (from SIR-C) for the scene (April 15, 1994) with selected crops.

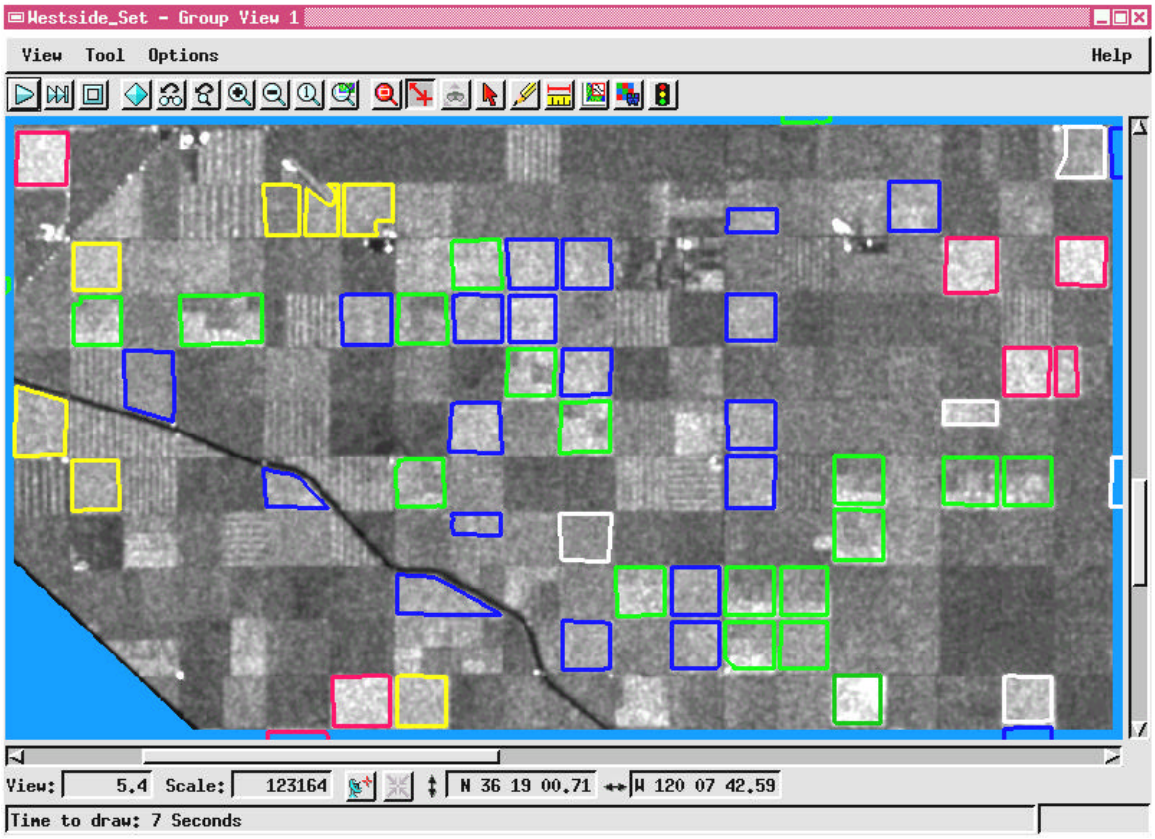

"VV" indicates that vertically polarized (first V) microwaves illuminated the scene and that the receiver was also sensitive to only vertically polarized (second V) microwaves in the returning echo. RADARSAT uses HH (horizontal polarization for both transmit and receive), but the C-band HH image (not shown) is quite similar to the C-band VV image.

Figure 6. TNTmips Histogram Display tool for C-Band VV (SIR-C) for April 5, 1994.

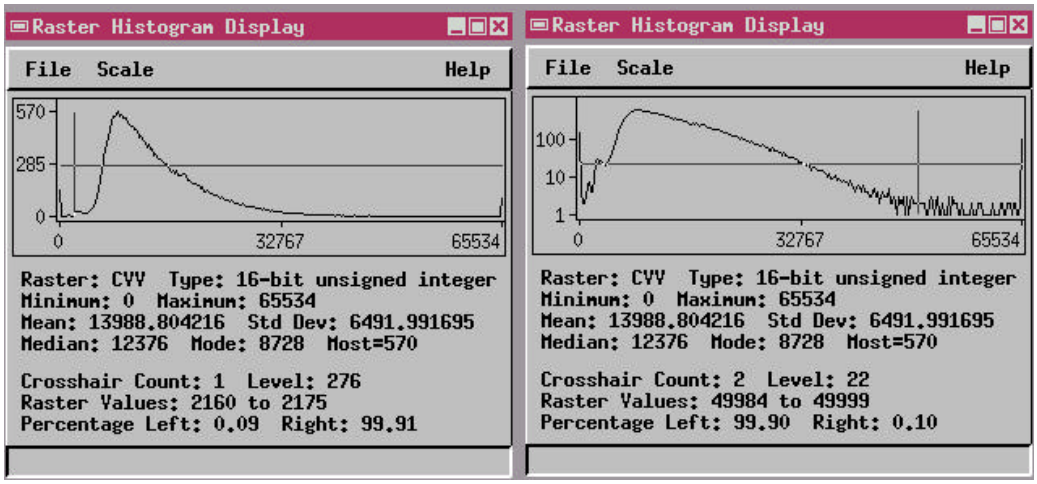

Crosshairs above indicate the 0.1 and 99.9 percentile levels. Note that I used a 16-bit unsigned integer for the C-band VV image raster (rather than a 8-bit unsigned integer). The radiometric resolution of SAR image data is significantly greater than for digital optical data. While some use 32-bits, this is overkill for SAR rasters. TNTmips can handle any bit-level raster. Note that the C-Band VV image is highly skewed. But, the skew is not so extreme that one needs to convert the brightness scale to a log scale [i.e., to decibels (dB), as is often used with SAR data]. I prefer to keep SAR data in non-dB (i.e., linear) brightness scales so that normal GIS/IP software functions can be used (e.g., low-pass spatial filtering).

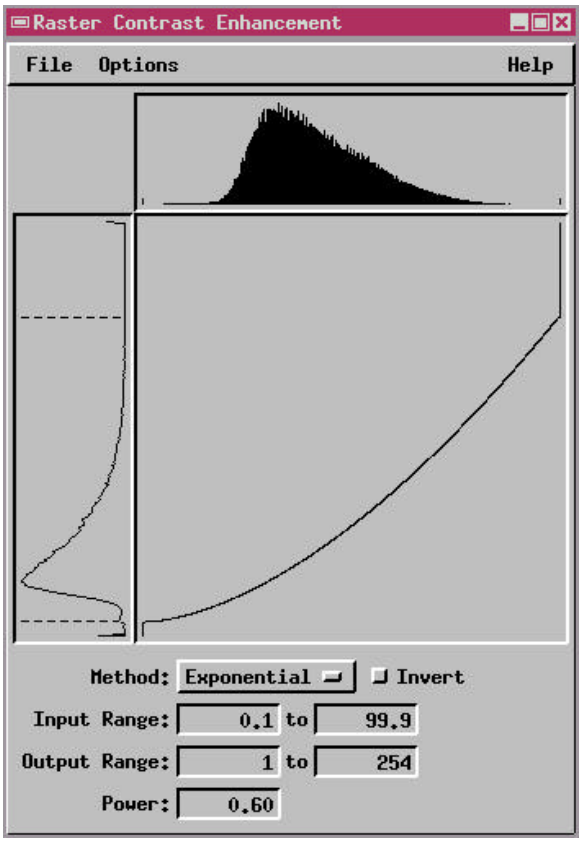

Figure 7. The TNTmips Raster Contrast Enhancement tool for the C-Band VV raster.

The contrast enhanced display of the C-band VV image in Figure 5 is similar to that used for the more common TM image. The main difference is that the TNTmips' look up table for a 16-bit (or 32-bit etc.) raster has 4096 bins, rather than only 256 bins. The looked-up (i.e., displayed) value is still in the range from 0 to 255. I still avoid 0 and 255 so that these may be used a null values (indicators of missing or transparent raster cells in a process or multi-GIS-layer view. Due to the skew of SAR data, I did "bend" the look-up curve more by using 0.6 for the power (rather than (0.7 as was used for the TM image).

Agricultural Information in the C-Band VV Image

Looking back at Figure 5, several characteristics can be noted. First, a primary driver for the brightness of this shortwave SAR image is terrain-feature roughness. The water in the California Aqueduct is smooth; therefore, the C-band VV backscatter is low (low magnitude echoes). Fields containing dense leafy biomass are moderately bright. Note the brightness of the sugarbeet fields (■), of most of the lettuce fields (■), and of the garlic (■) and onion (white) fields. The cabbage field is especially bright (■). Those familiar with the radar backscattering properties of trees might be surprised to see the not-so-bright appearance of the orchards and vineyard (■). Recall that C-band is relatively short for a microwave band; the leaves in the orchards and vineyards are dampening the backscattering from the branches due to absorption of microwaves by the leaves. I observed this effect in controlled field investigations with a C-band truck-mounted scatterometer when viewing plum trees undergoing leaf expansion and growth in this period of time. A few bright spots exist in Figure 5. These are buildings (mostly metal) that exist in the area.

More than roughness and biomass differences are seen in Figure 5. Many of the bare fields (outside of the colored polygons) have bright striping patterns. These are caused by the fact that strip irrigation is a common practice in this region of irrigated agriculture. The bright lines in the C-band VV image coincides with the dark lines in the TM Band 3 image. Recall that these two images are 10 days apart in time (Figure 2 is April 5, 1994, and Figure 5 is April 15, 1994).

Figure 8. L-Band VV image (from SIR-C) for the scene (April 15, 1994) with selected crops.

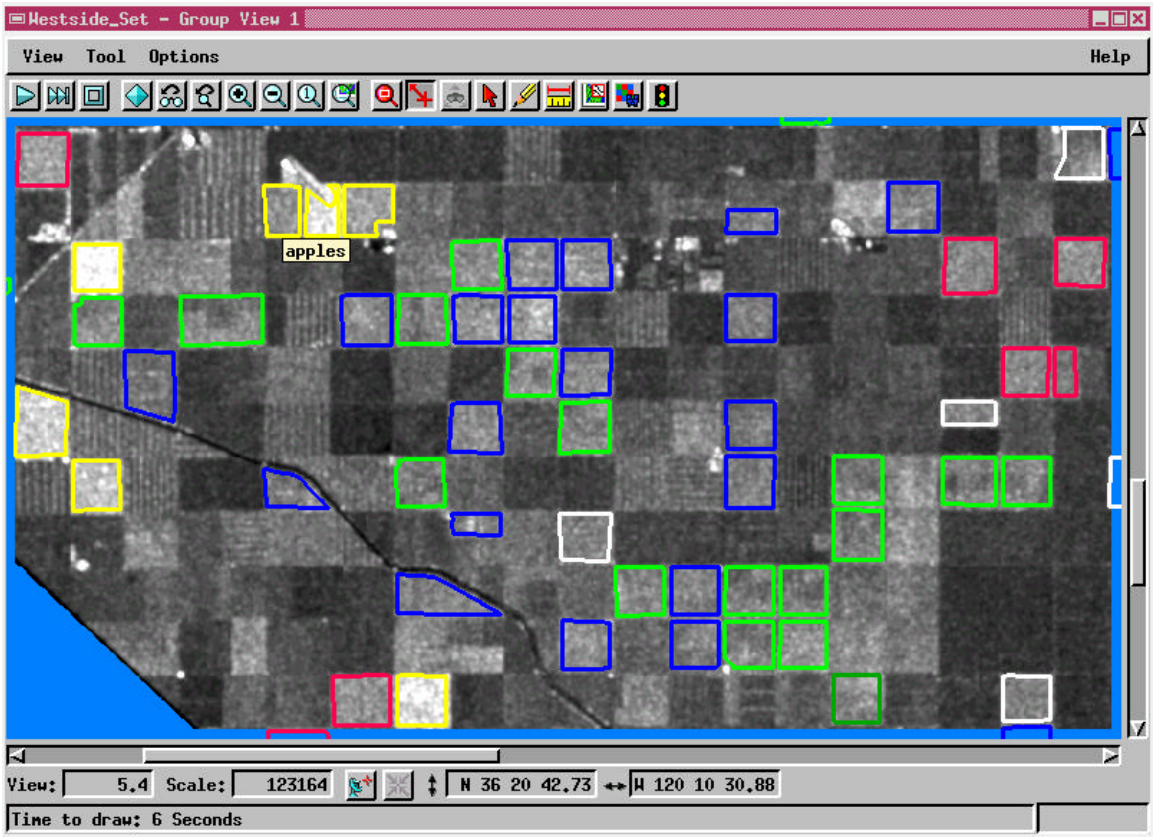

The wavelength for L-band is about 24 cm (compared to the 6-cm wavelength of C-band). This is a drastic change in wavelength, and it is accompanied by drastic changes in backscattering (for some terrain features). The smooth, open water in the California Aqueduct stays dark (as it was for C-band. Many of the bare fields are darker now (than they were for C-band). Most of the orchards have become quite bright. This is due to the fact that the leaves on the trees in these older orchards have become more transparent; thus, the brighter branches show through. Employing a very useful tool in TNTmips, called the DataTip (a popup that shows you the content of a record of a selected field in a database associated with a GIS vector element being pointed to), I have pointed out the two apple fields (above the DataTip). The apple orchard on the left (west) is much younger than the one on the right (east). The wine-grape vineyard, by the way, is east of the older apple orchard. The rest of the orchards (■) are almond orchards that are in full leaf by the time of this April image set. Note that the L-band VV brightness of these four almond orchards varies from one to the other. The differences are primarily in the above-ground biomass. However, there is an effect of the density of trees that affects the ability of microwaves to penetrate through gaps in the canopy. Penetrating microwaves can interact with both the branches and/or trunks and the ground in a double-bounce, corner-reflecting way. This enhances the HH scattering. Finally, the same stripped irrigation patterns are seen with wet strips being brighter than drier strips (as was the case for C-band VV) (Benallegue *et al.*, 1995).

The histogram for this L-band VV image (and the corresponding contrast look up table) – both not shown – are similar to the one shown for C-band VV. However, the skew is stronger; thus, the look-up curve has to be "bent" more to center the displayed brightness.

This skewness is due partly to the fact that woody vegetation and vegetation having larger plant-part sizes will be more efficient in backscattering L-band as compared to C-band (Paris and Kwong, 1988). Also, the bare surfaces are darker at L-band than at C-band due to change in

wavelength compared to absolute departures in surface variations. This drives part of the scene to lower values. Thus, a wider distribution is seen in L-band. Nevertheless, the standard Contrast Enhancement Tool in TNTmips can handle this situation.

Effects of SAR Polarization

I am still looking at monospectral RS images for the selected scene. In the case of SAR, it is possible to employ a few different polarization combinations, as follows:

VV	Vertical transmit, vertical receive
HH	Horizontal transmit, horizontal receive
VH	Vertical transmit, horizontal receive
HV	Horizontal transmit, vertical receive
RR	Right-hand circular transmit, right-hand circular receive
LL	Left-hand circular transmit, left-hand circular receive
RL	Right-hand circular transmit, left-hand circular receive
LR	Left-hand circular transmit, right-hand circular receive

VV and HH as well as RR and LL are called like polarization combinations (LK). VH, HV, RL, and LR are called crossed polarization or just cross polarization combinations (CS).

In addition to these various magnitude combinations, one can also make an image out of the electric phase differences between two polarized echoes. Phase is how engineers and scientists characterize the oscillating nature of coherent electromagnetic radiation like those used in SAR. For a single (mono) parameter SAR system, the phase acts like a random variable. However, it is really being driven by the interactions among various and numerous point sources of backscattering with due regard to their precise locations in 3D space. If, however, you compare the phase of a VV echo with the phase of a HH echo, you get non-random (i.e., meaningful image data). This is called a phase difference (PD) image. This appears to be interesting only for the phase difference between HH and VV. So, I call this the like-polarization phase difference, PDLK or just PD (since cross-polarized phase differences do not appear to be useful). Phase difference (PD) varies in a circular function from –180 degrees to 0 degrees to +180 degrees, (which is the same as –180 degrees on the PD circle).

There are many controlling factors involved in the determination of PD. One is the number of interactions (number of bounces). An odd number (usually one) of bounces produces a PD of zero degrees. An even number (usually double bounce) of bounces produces LKPD values near –180 or near + 180 degrees (opposite side of the phase difference circle). A useful image, then, is the *absolute value of the PD*, or |PD|. This is shown later. Before this, I present HH and CS images for the SIR-C L-Band data set for April 1994.

Figure 9. L-Band HH image (from SIR-C) for the scene (April 15, 1994) with selected crops.

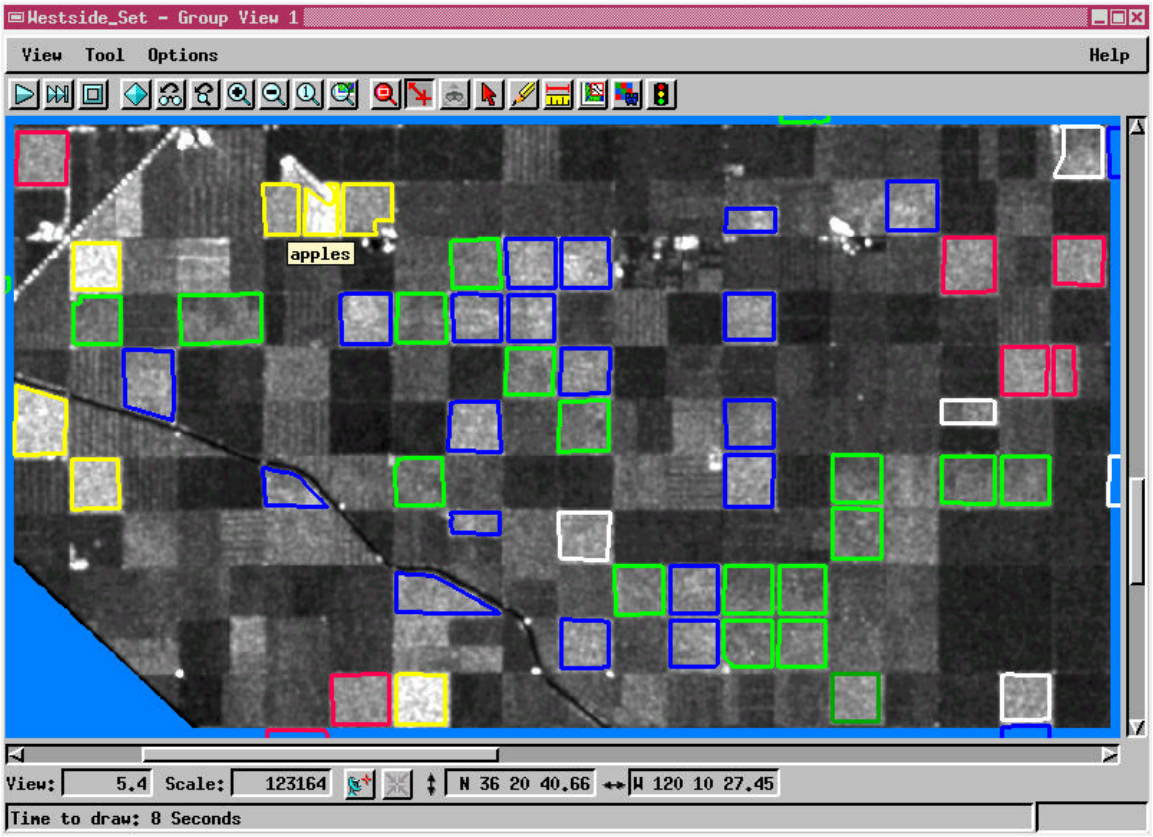

A close inspection of this figure (compared to Figure 8) will reveal some small differences between HH (and VV). But, for the most part, the VV and HH images are the same.

In this HH image, the well-known effects of coherent interference can be seen. This is present in all SAR image data, especially those that have not be spatial averaged to reduce this characteristic of SAR image data. This brings up an difference between SAR and optical images. For an optical image, the spatial resolution is well represented by the pixel cell size. But, for SAR, a high-resolution SAR image with coherent interference (scintillation) does not allow a user to identify terrain features that might otherwise be seen at the high resolution. Low-pass filtering will reduce speckle at the cost of lowering the spatial resolution. So, a one-meter monospectral SAR image may behave more like a 5-10 m image in terms of terrain feature recognition.

Figure 10. L-Band CS image (from SIR-C) for the scene (April 15, 1994) with selected crops.

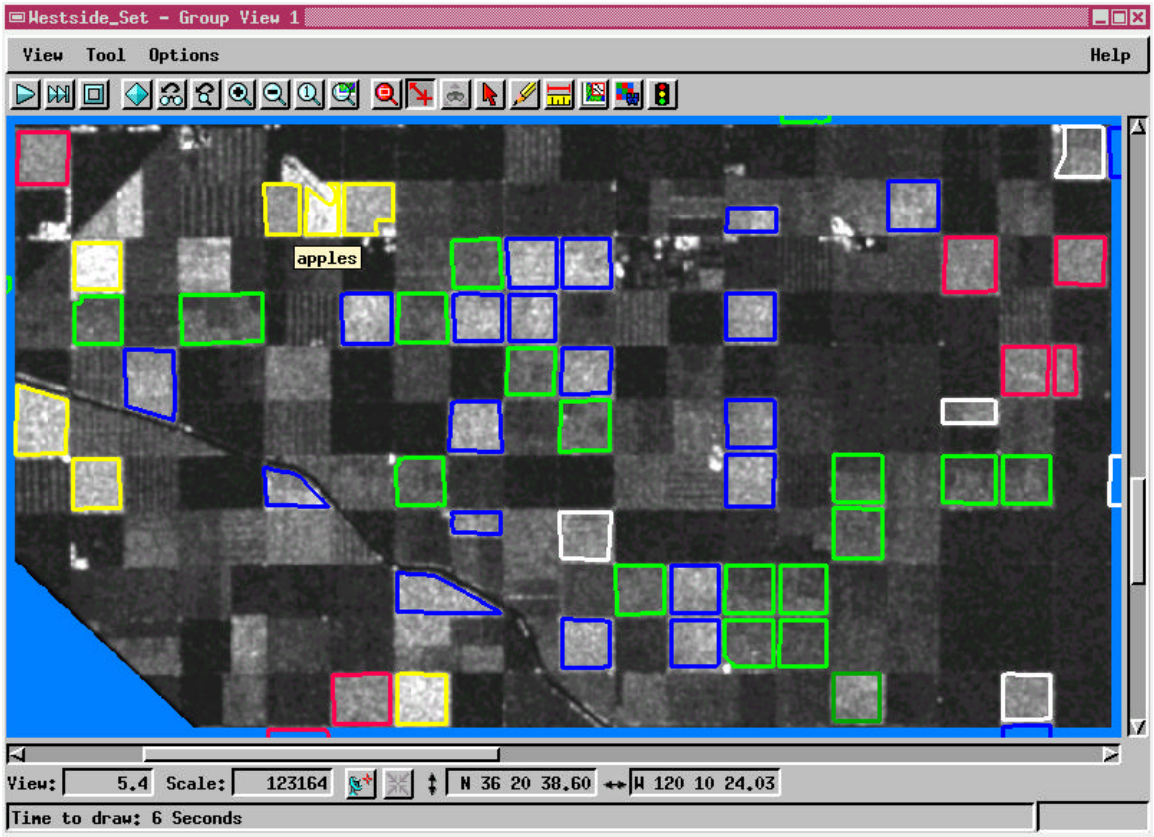

The enhanced L-Band CS image above looks similar to the VV and HH images at the same wavelength. A few bright corner-reflecting features, seen in the HH image along the California Aqueduct, have disappeared in this CS image. They were also less prominent in the VV image. So, for this scene that has most annual crops and low biomass orchards, all three L-Band magnitude images are about the same (except for overall levels of backscattering for each).

In other vegetation contexts, e.g., in heavily forested scenes, CS is clearly superior to HH or VV as an indicator of woody biomass. This just is not the case in this predominately agricultural scene.

Regarding image speckle, this is less in a CS image (than in the corresponding HH or VV image) due to the fact that two independent CS images (VH and HV) are merged into one as an average CS image. Also, CS images tend to be dominated by multiple scattering processes that reduce, somewhat, the interference effect.

Figure 11. L-Band |PD| (absolute value of PDLK) image (from SIR-C) for the scene (April 15, 1994) with selected crops.

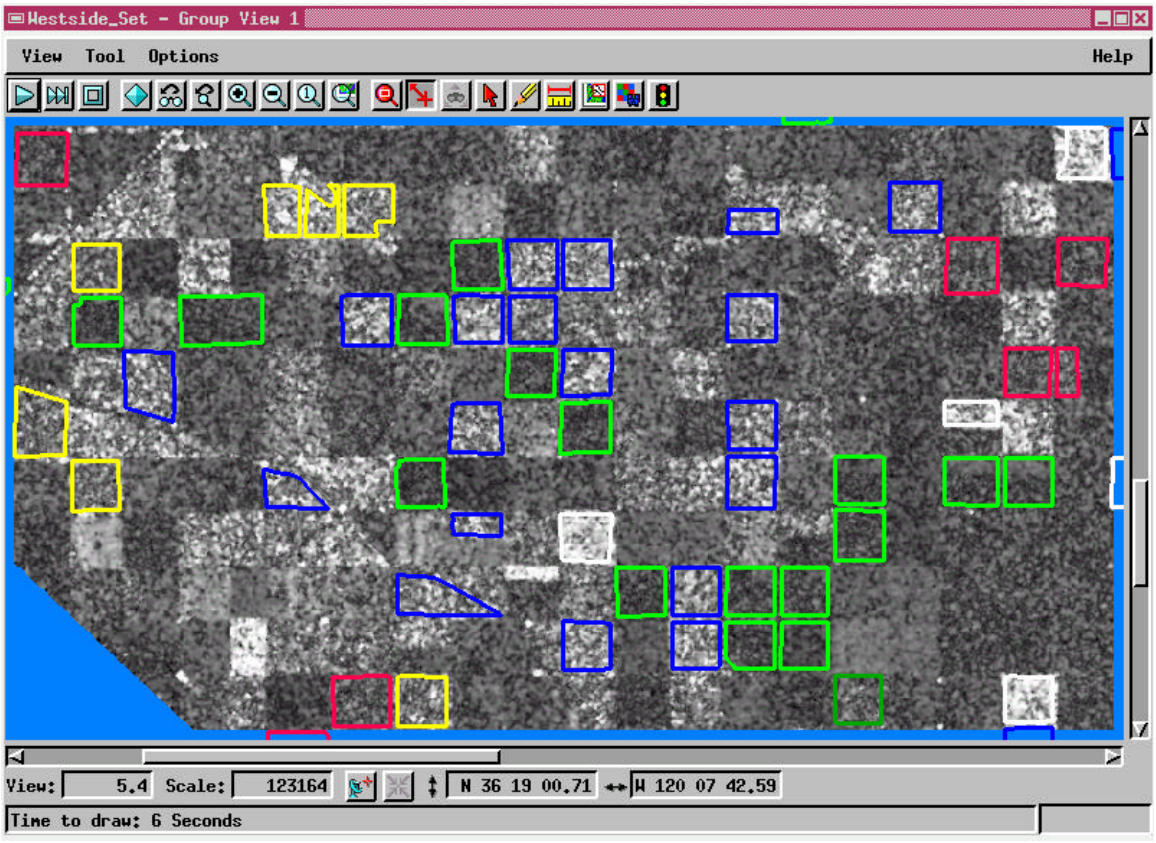

The above image of |PD| is a noisy and bizarre image. The bright pixels in this scene are those in which double-bounce interactions are dominate. Note that this occurs mostly in onion fields (white). Double bounce is dominant also in garlic fields (■), Dark pixels (single bounce) occur in crops like sugerbeets (■) and lettuce (■). Onions and garlic have vertical stalks (that encourage double bounce interactions) while sugarbeet and lettuce lack this structure (that encourages single bounce interactions).

There is still much to learn about how SAR images can be used for agriculture. It is clear, however, that some important kinds of information needed for the crop risk insurance industry can be extracted from every monospectral SAR data, especially if the effective spatial resolution is high (from 3 to 10 m, after speckle reduction). The continuing LightSAR program should add much to the understanding of these issues.

Returning to the Monospectral Optical Case

So far in this paper, I have been considering possible uses of monospectral RS image data, both for the optical and for the microwave (radar, SAR). As most everyone knows, there are not too many proponents of using monospectral RS image data for agriculture applications beyond the relatively simple use for field mapping.

Using Changes Over Time in a Monospectral RS Data Set

There is, however, the possibility of having using changes over time in a monospectral RS set to infer changes in crops over time, especially if the crop type is known. In the case of precision farming applications of RS, the crop type is known to the end user of the data. If so, then the issue is to what degree growth information and/or growth problems can be gleamed from a time series of monospectral RS data. In particular, I want to consider the case before us in the example project used in this paper.

The question that can be posed is as follows: What information can be extracted from having two closely spaced dates of monospectral RS data (e.g., TM Band 3 on April 5, 1994, and again on April 21, 1994)?

The TM Band 3 image for April 5, 1994, has already been presented in Figure 2. Recall that the best estimate for the calibration parameter, V_p (representing path radiance in the scene) for TM Band 3 for April 5, 1994, is 19. This is the minimum value for the raster that contains dark objects such as the water in the California Aqueduct and dense tree vegetation in the West Side Experiment Station. Lacking a terrain object of known reflectance, we cannot determine the other calibration parameter, m. There is a technique that may yield this value, but it involves the use of the near infrared (NIR) with the red-light (RL) image as a dual-band multispectral (MS) data set. I am still discussing monospectral approaches here.

The minimum brightness value for the April 21, 1994, TM Band 3 raster (Figure 12, next page) is 23. This change over 16 days is due to a combination of the changing solar elevation angle [i.e., the cosine effect of Eq. (1)] and possibly higher levels of dust on April 21, 1994. In any case, a good estimate of V_p for TM Band 3 for April 21, 1994, is 23.

So-called raster algebra, such as in the TNTmips Raster Combination (Predefined) process, can be used to subtract V_p from each V value to make a set of rasters that no longer contains the additive effects of path radiance. To some, this first step of processing may be obvious. However, I have seen more errors in this regard than not in dealing with many end users of RS data. There really is no excuse for not estimating the brightness equivalence of path radiance and then subtracting this from the original optical raster. Most end user know to set a minimum level for displaying a raster at or near this path-radiance equivalent brightness value, but many do not know that this should also be done in numerical processing of a raster or rasters for quantitative information extraction.

With path radiance subtracted, one is left with a set of new raster values – N_t and $N_{t+\Delta t}$.— for the same wavelength band. In terms of R,

$$R_t = m_t N_t \text{ and } R_{t+\Delta t} = m_{t+\Delta t} N_{t+\Delta t} \qquad (5)$$

Thus, for objects that have the same reflectance for both dates, the ratio ($R_{t+\Delta t}$ / R) of path-corrected raster values (N) are related by a constant multiplicative factor, $m_{t+\Delta t} / m_t = r$. There are usually a number of terrain objects in a scene that are invariant, especially over short periods of time. This would include features such as dry dirt roads, level roof tops, some soils, and paved roads. If two raster sets (monospectral or multispectral) have been registered, then they may be warped (resampled) to overlay each other in cell size, orientation, and extent. Then, a raster to

raster correlation tool (e.g., the TNTmips' Raster Correlation tool in Geospatial Data Display) can be used to determine the relative multiplicative factor needed to correct one raster set to match the other. Furthermore, standard multispectral classification tools can be used with the corrected multi-date, monospectral set to determine quantitative changes over time that track changes that have occurred in reflectance. Let's look at the specific example.

Figure 12. TM Band 3 for the area shown in Figure 1, but for April 21, 1994.

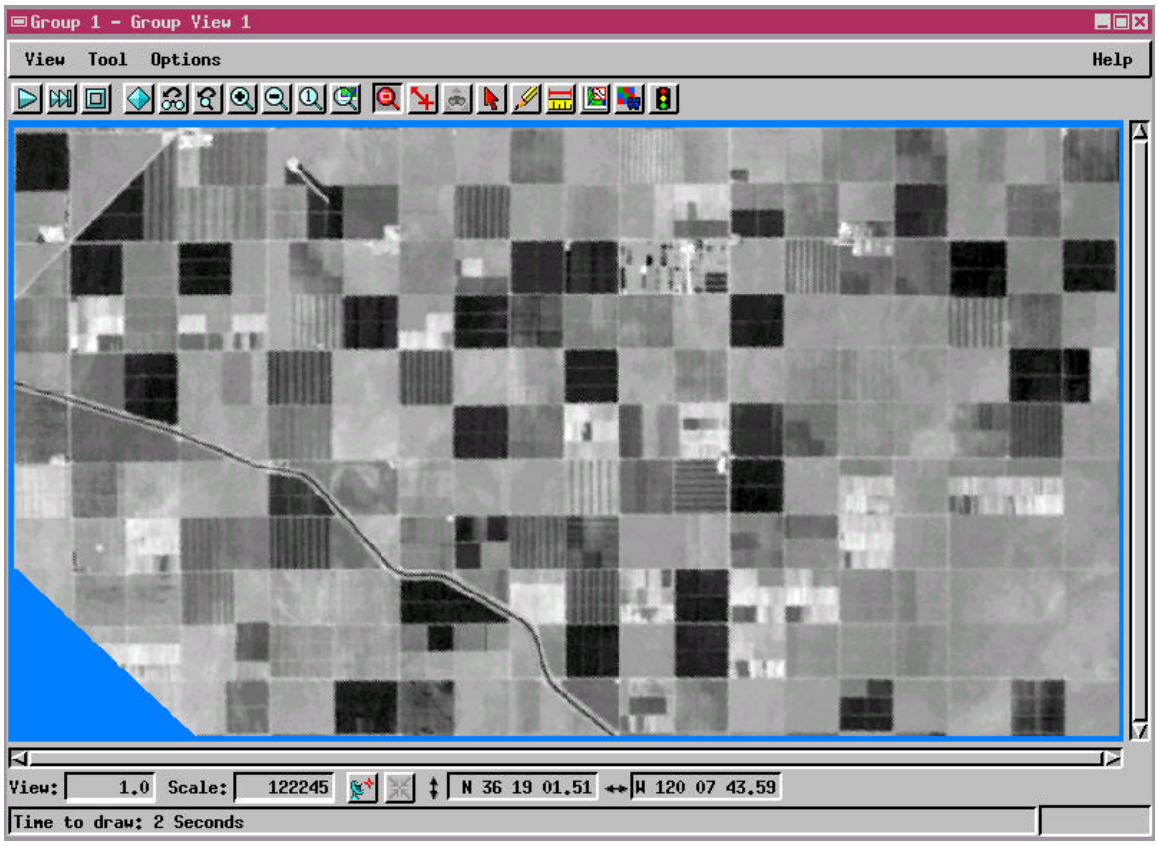

In the case of this scene, an invariant object exists just north of the two apple orchards – a landing strip for small aircraft. The ratio of the corrected raster values for this object is 1.064815. So, multiplying the path-corrected April 5 data by this factor will allow one to compare these to the April 21 data. Note that is done without knowing the absolute radiometric scaling factor for either date (i.e., without an estimate of m for each date).

I perform this relative rescaling operation using a TNTmips process. Then, I can use several techniques to display or to quantify the changes from pixel to pixel between the two dates (all for TM Band 3, of course).

One method is to use an RGB (additive red, green, blue) display with G used for the corrected April 5 data and with R and B each used for the corrected April 21 data. This choice is made so that areas that decrease in red-light corrected brightness (between the two dates) will be greenish and areas that increase in red-light brightness (over time) will be magenta-ish. Areas of no change should be shades of gray – i.e., bright areas remain bright and dark areas remain dark.

Figure 13. Using an additive RGB for relatively-corrected monospectral band image data to indicate areas of qualitative change: April 5 as G and April 21 as R & B (magenta).

The figure shows clearly that the use of multi-date data is powerful even when no multispectral data are used. I have added a new class of fields – tomatoes – as indicated by the fields outlined in orange. These plants have just started emerging by April 21, 1994. The use of the red-light only band and changes over time is able to track this emergence.

Multispectral Optical RS

This topic has received a great deal of attention over the past several decades (Clevers, 1988; Crist, 1985; Huete, 1986 & 1988; Kaufman and Tanre, 1992); Tucker, 1979 – to cite just a few references). Multispectral RS (MS RS) has been a generally successful technique for general vegetation analyses. The advent of the Landsat Multispectral Scanner System (MSS) in 1972 spurred many RS scientists to develop a whole host of MS approaches. These are all covered well in the many standard RS textbooks.

Now, there are many MS RS systems including the Thematic Mapper (TM) on Landsat 5, the LISS (like TM) on the Indian Remote Sensing Satellite (IRS), and the SPOT XS. These MS RS systems all contain a red-light (RL) and NIR band – the minimum two bands required for single-date vegetation work. Even the AVHRR imager on today's weather satellites has both RL and NIR with 1-km pixels. The new Vegetation sensor on SPOT 4 is similar to this coarse resolution mapper. In addition to the many satellite-based RL-NIR MS RS systems, there are uncountable aircraft-based systems. The most common aircraft-based system is a four-band imager that includes blue light (BL), green light (GL), RL, and NIR. Typically, such digital systems yield 1-2 m spatial resolutions and offer quick turn around of digital products. Some of these go so far as to

be turned into GIS-ready MS RS raster sets with calibrated reflectance (or at least date to date adjustments like the dual date TM Band 3 set that I have just finished covering.

You would think that nothing much new could be written about RL-NIR RS. But, every issue of any of the leading RS journals still contains new uses of old algorithms or new ways to develop indices of vegetation based on the TM shortwave bands or a subset (down to RL & NIR only).

Using the Common NDVI Approach

The USAID's Famine Early Warning System (FEWS) posted this interesting message on their Web site:

Hopefully, my discussion below will help you understand why using the popular NDVI maps might be hazardous to your conclusions. Let's look into this issue.

The most used and abused RS-derived index is the Normalized Difference Vegetation Index (NDVI). This has been used especially used by Tucker (1979). You can easily find NDVI maps on the Web (e.g., *http://www.agribiz.com/*).

Technically, NDVI is defined as:

$$NDVI = (R_{NIR} - R_{RL}) / (R_{NIR} + R_{RL}) \quad (6)$$

Note that you should use reflectance, R, in Eq. (6), not raw raster brightness values. Unfortunately, many who claim to be using an NDVI approach to vegetation mapping are wrongly using raw raster values and not reflectance. This problem, I believe, stems from another often-given informal definition for NDVI, namely, NDVI = (NIR – Red) / (NIR + Red). I have seen some investigators use the NDVI formulation with digitized aerial photography where the "Red" and "NIR" values are the digital (raw) outputs of some RGB scanner that has operated on color infrared (CIR) film (prints or transparencies). The abuse here is that there is a non-linear relationship between the scanner output and the radiance of the scene. As serious, is the fact that red light exposes both the magenta-forming (green looking) emulsion and the cyan-forming (red looking) emulsion in CIR film. NIR radiation, at least, does expose only the cyan-forming (red looking) emulsion in CIR film. But, the distribution of red light among the G and R primary colors in a typical positive color CIR image is a serious problem when it comes to trying to do spectral analysis. Mixing the wavelengths into one of the dye components is an irreversible process that contaminates the information extraction process.

If you carry the calibration parameters, $\mathbf{V_p}$ and **m** into Eq. (6), you get an expression for NDVI in terms of V (V_{NIR} and V_{RL}) that cannot be scaled into the correct values of NDVI that would arise from using actual calibrated reflectance. First, the path-radiance offsets must be subtracted. Then, you should scale the path-radiance corrected raster values (at least in a relative sense) to reflectance before calculating NDVI. It is difficult to determine whether or not this process was followed in creating the many NDVI maps you can find now on the Web and in other publications.

Another aspect of NDVI that is often ignored is that it is negative for half of the NIR-Red feature space (where R_{NIR} is less than R_{RL}). Look at how NDVI values plot out in NIR-Red feature space. This can be seen with the use of the TNTmips Raster Correlation tool with the use of TM Band 3 and TM Band 4 from the April 21, 1994, data set in my model project (see Figure 14, next page).

Figure 14. Scatterplot of pairs of TM Band 4 (NIR) versus TM Band 3 (RL) for data acquired on April 21, 1994, in the selected illustrative site.

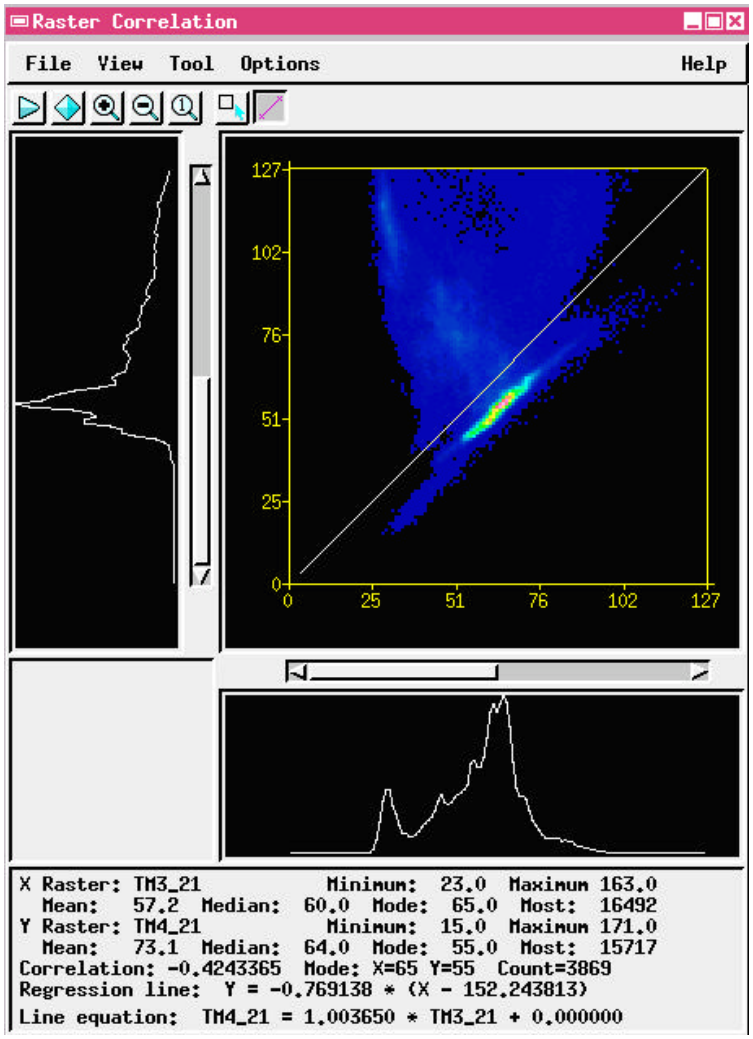

This TNTmips two-dimensional spectral feature space plot uses color to indicate the density of points in the space. Black areas are spectral combinations where no NIR-Red pairs exist. Dark blue areas are populated by at least one pair. Colors from dark blue through cyan to green to yellow to red and finally to bright magenta indicate increasing concentrations of spectral combinations that exist in the two image rasters.

Since the illustrative test site has a large number of bare-soil pixels, high concentrations of the spectral points are found along a line (Line of Bare Soils) where the NIR brightness is positively correlated with the RL brightness. Note the blue pixels that extend toward dark values in both spectral bands; these are associated with the clear water in the California Aqueduct.

As green vegetation emerges from bare soil, the spectral signature moves from the Line of Bare Soils toward a region in the plot where NIR brightness is high and RL brightness is low. The changes in NIR brightness are caused by the build up of leaves that are brighter than the background soil in the NIR. The changes in RL brightness are caused by the absorption of RL by chlorophyll in the leaves. When the green cover reaches 100%, the RL brightness reaches a minimum while the NIR brightness continues to rise (for herbaceous plants) as green leaf area grows. When 100% covering green leaves turn yellow (i.e., lose chlorophyll), the RL brightness increases while the NIR brightness stays at high levels. The process continues (in some cases) until the changes bring the spectral trajectory back to and even across the Line of Bare Soils. Thus, yellow leaves and litter co-exist on the Line of Soils with high brightness in both NIR and RL. Manmade materials (e.g., roof tops and roads) tend to have spectral plots below the Line of Bare Soils.

It is important to know have NDVI changes from place to place in this diagram. Along the RL axis (x-axis), NIR is zero, but RL is not. Thus, NDVI = -Red / Red = -1 on this axis. Along the diagonal (shown as a white line in Figure 14), NIR is equal to RL. Thus, the difference between NIR and Red is zero, and NDVI is 0. Along the NIR axis (y-axis), RL is zero, and NIR is not. Thus, NDVI = NIR / NIR = +1 on this axis.

In some software, the NDVI expression is used with a multiplicative scaling factor (e.g., 255). The output raster for the resulting NDVI calculation process is an 8-bit unsigned integer raster.

Therefore, it can only have positive values from 0 to 255. Any spectral plots that fall below the diagonal line in Figure 14 would be negative and therefore would be assigned to the lowest allow value, 0. Note that the uncalibrated brightness values associated with the Line of Bare Soils all fall below the diagonal line. Thus, all soil pixels in the related scene would have NDVI values of 0. As green vegetation grows, the spectral signature of the affected pixels moves towards the upper left-hand corner of the plot. Note that some green growth much occurs before the spectral point crosses the diagonal line to go into positive territory in the plot. One RS company who was (and still is) developing an MS RS based service for precision ag from space came to me one time and noted that the NDVI was not detecting newly emerged corn. It turned out that the location of the Line of Bare Soils was similar to that shown in Figure 14. Thus, the spectral plot for the growing, green corn had to move some distance in negative NDVI space before the values became positive and "the growing corn was detected." This example shows the importance of calibrating both the NIR and the RL bands, at least to relatively correctly reflectance before NDVI is calculated.

A better way to calculate an NDVI-like raster is to use the proportion index (PI) involving two rasters, A and B, as follows (Crippen, 1990):

$$PIBA = B / (B + A) \tag{7}$$

If B represents R_{NIR} and if A represents R_{RL}, then it is easy to show that PIBA and NDVI have a linear relationship. Let NDVI = (B – A) / (B + A).

$$\begin{aligned}(NDVI + 1) / 2 &= \{[(B - A) / (B + A)] + 1\} / 2 \\ &= \{[(B - A) / (B + A)] + [(B + A) / (B + A)]\} / 2 \\ &= [2\ B / (B + A)] / 2 = B / (B + A) \\ &= PIBA \end{aligned} \tag{8}$$

I have used the PIBA formula in many RS contexts – both optical and SAR. Note that if B is zero, then PIBA is zero. In addition, if B is equal to A, then PIBA = 0.5. Also, if A is zero, then PIBA is 1. So, it is easy to make an 8-bit unsigned integer raster by using 1 + PIBA * 254. This reserves the value of 0 for situations where A and B are both zero (or where both A and B are close to zero where integer values of A or B have an unreasonable effect on PIBA.

It is possible to use the PIBA function on relatively uncalibrated data so long as the path radiance values have been subtracted (as was done earlier in this paper). Nevertheless, it is better to scale either NIR or RL rasters to achieve relative calibration. This can be done by taking advantage of the known value of the slope of the Line of Bare Soils. For a sandy loam soil, for example, this ratio slope is 1.152. Note that the Line of Soils does not pass through the spectral (feature space) origin. Rather it, intercepts the NIR reflectance axis at 5% reflectance. This presents a dilemma. The PIBA (or NDVI) formulation is a series of isolines that pivot on the point where both reflectances are zero. In uncorrected raster value space, it pivots on the point defined by the two path-radiance raster values. But, since the Line of Bare Soils does not pass through the PIBA or NDVI pivot point, then PIBA and NDVI will change along the Line of Soils due to changes in overall soil brightness (in all bands). I recommend that one force the PIBA formulation to coincide with the Line of Bare Soils for one of the isolines. Given that the pivot point is not at the path radiance point, there will be an effect of land terrain slope and aspect on the calculated values. However, since most of cropland is on gentle slopes, this should not be much of a problem for cropland applications of NDVI nor of PIBA.

Let me proceed now with an example of the use of PIBA with TM data from the sample project.

I used the TNTmips Raster Correlation tool for both the April 5 and April 21 (1994) TM data (Bands 4 and 3 for NIR and RL, respectively) to view a feature-space plot for each date as shown in Figure 15.

Figure 15. Feature space plots for April 5 (left) and April 21 (1994) for TM Band 4 versus Band 3 for the illustrative study site.

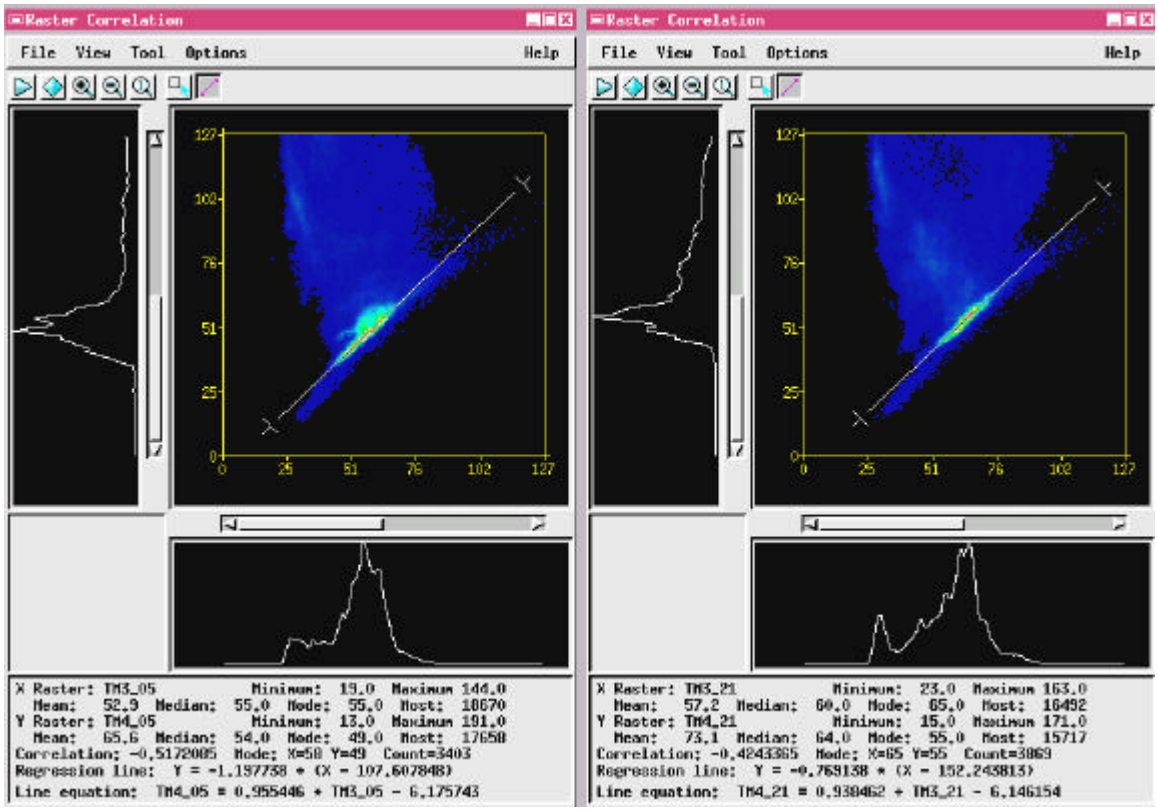

The recommended PIBA pivot points are shown in the two plots as the dark end of the white diagonal line (running through the Line of Bare Soils). For April 5, 1994, the pivot point is RL = 18 and NIR = 12. For April 15, 1994, the pivot point is RL = 22 and NIR = 14.

TNTmips has formulated the PIBA process (called Modified ND) into its Raster Combine options. In this version, you can specify the path radiance values (i.e., V_p) and calculate the PIBA for the path-radiance-corrected values – all in the same processing run. I used the parameters given above to do these calculations for the scene for both dates.

Figure 16. Contrast Enhancement tools showing histograms of calculated PIBA rasters (vertical axes) and the use of a look up table to convert PIBA to Green Cover (GC, %).

April 5, 1994 April 21, 1994

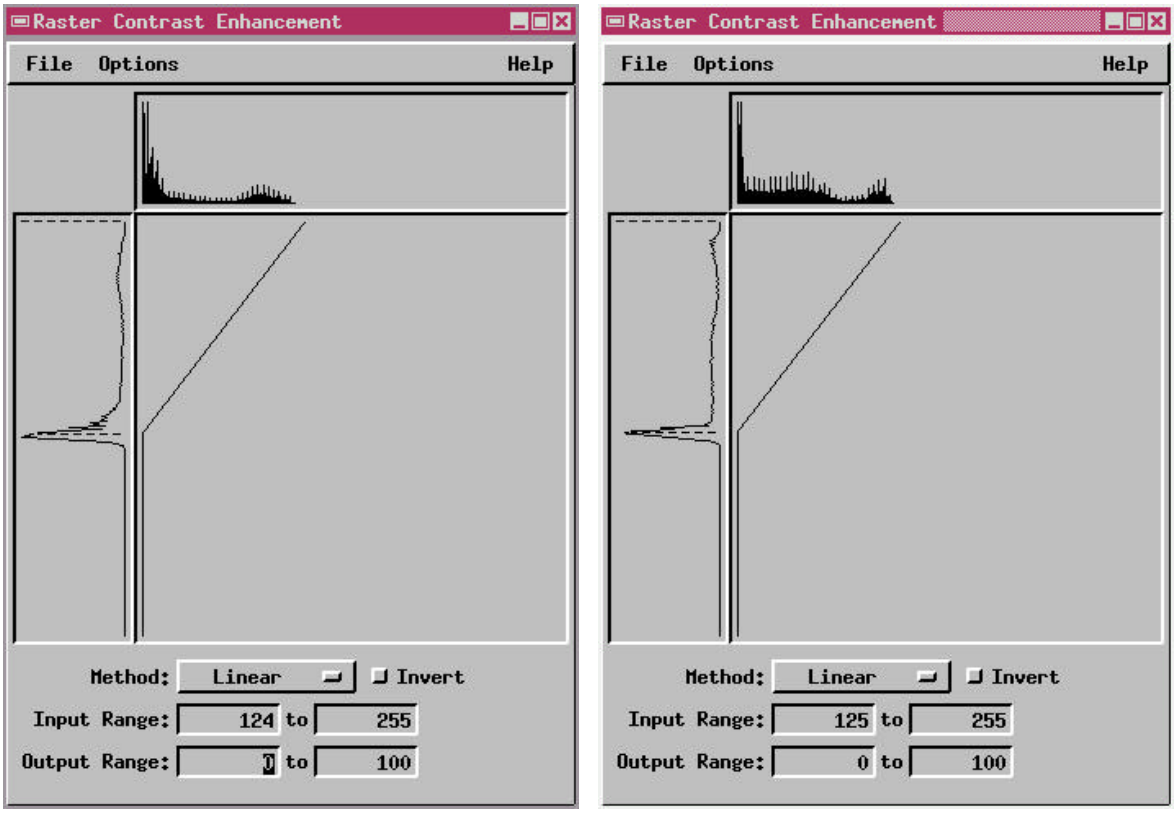

Note that if the pivot point for the PIBA algorithm is designed to be at the intersection of the Line of Bare Soils and the line where R_{RL} = 0%, then the Line of Bare Soils reduces to a Point of Bare Soils (PBS) in the PIBA image. In the specific case above, PBS was 124 for April 5, 1994, and was 125 on April 21, 1994. It is logical to assume that the Green Cover (GC) at the PBS point is 0% and that GC is 100% at the maximum value of PIBA (i.e., at 255). The look up tables takes these two extreme points and scales them to a 0 to 100 (%) range. Thus, a GC raster can be produced for each date.

The GC values are calibrated biophysical interpretations of the original TM Band 3 and TM Band 4 data. One way to display (present) the multi-date changes in GC is to assign the April 5, 1994, GC to R and B (in an RGB display) and to assign the April 21, 1994, GC to G. Increases in GC would then be indicated by shades of green and decreases in GC would be indicated by shades of magenta. Areas of no change would be shades of gray. Black areas are places where GC was low on both dates. White areas are places where GC was high on both dates. This display is shown in Figure 17 (on the next page).

Figure 17. Multi-date image of Green Cover (GC) rasters. GC for April 5, 1994, was assigned to R & B in the RGB display. GC for April 21, 1994, was assigned to G in the RGB display.

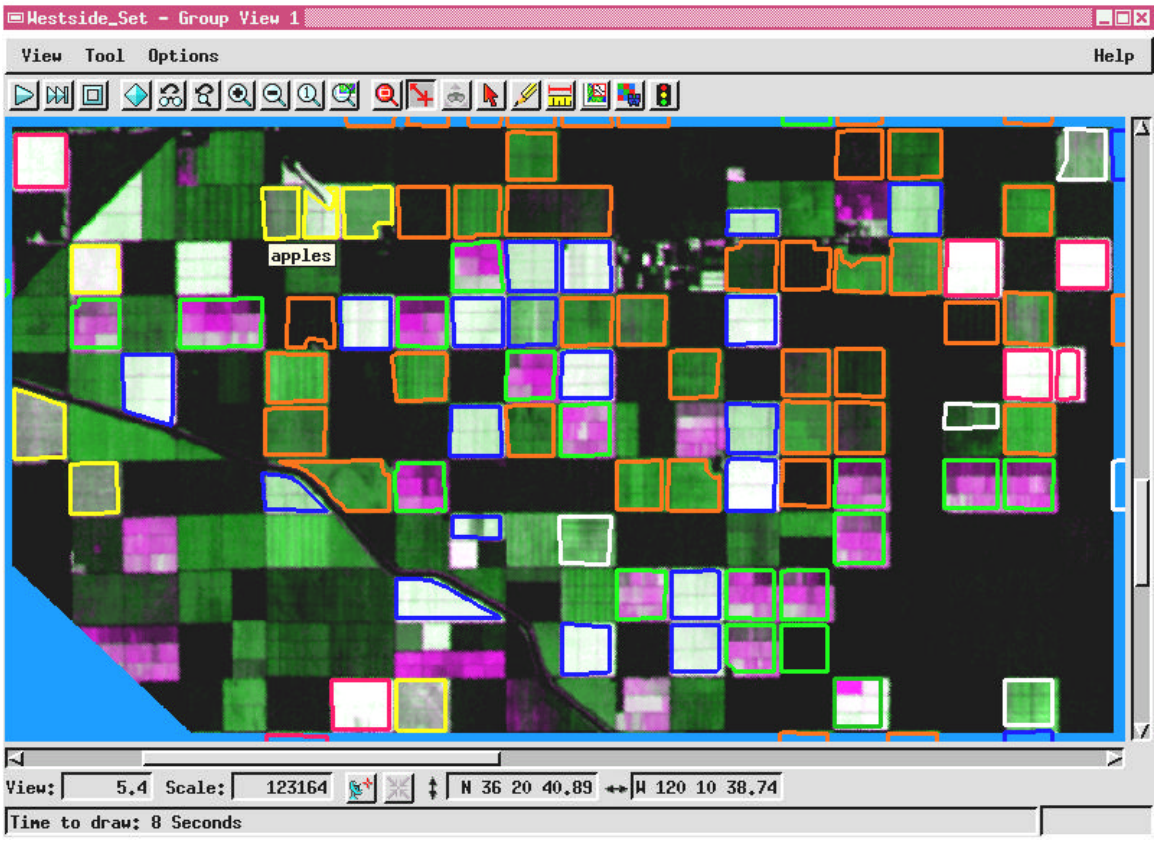

If you compare Figure 17 to Figure 13, it is easy to see how the weak information contained only in the red-light band (Figure 13) is enhanced by involving the near infrared band (Figure 17). Also, note that the disparate influence of wetness and dryness in the surface soils (see in Figure 13) are reduced in Figure 17. This is due to the fact that changes in surface soil wetness move reflectance up and down isolines of constant PIBA.

What Information is Lost in the NDVI / PIBA Approach

There is a down side to the use of a ratio index like NDVI or PIBA. Any information contained in the unique brightness of NIR or RL is lost in the ratio. For example, if you look at Figure 15, you can see that the NIR continues to rise beyond the point where GC (and PIBA o NDVI) has reached a maximum value. Also, neither NDVI nor PIBA distinguishes between dark points on an isoline (where crops may be early in the season as they grow) and bright points on an isoline (where crops may be late in the season when green leaves turn yellow).

To retain full information in a MS RS scene, you need to use all bands (hopefully converted to reflectance with due regard to path radiance). An example of this would be the use of TM Band 3 and TM Band 4 as reflectances. For example, if one were to do a cluster analysis of these two bands, then full information would be retained. A twist to this common approach would be to use two days of TM data (and two bands on each date) to generate clusters. The resulting clusters would have both MS properties and multi-date properties (Roberts *et al.*, 1993; Lyon, *et al.*, 1998). These results could be visualized in a two-dimensional feature space plot with lines connecting the spectral points (class centers) for the two dates.

Figure 18. Feature space plot of cluster centers (50 classes) based on April 5, 1994, and April 21, 1994, calibrated TM data (Bands 3 & 4 for both dates).

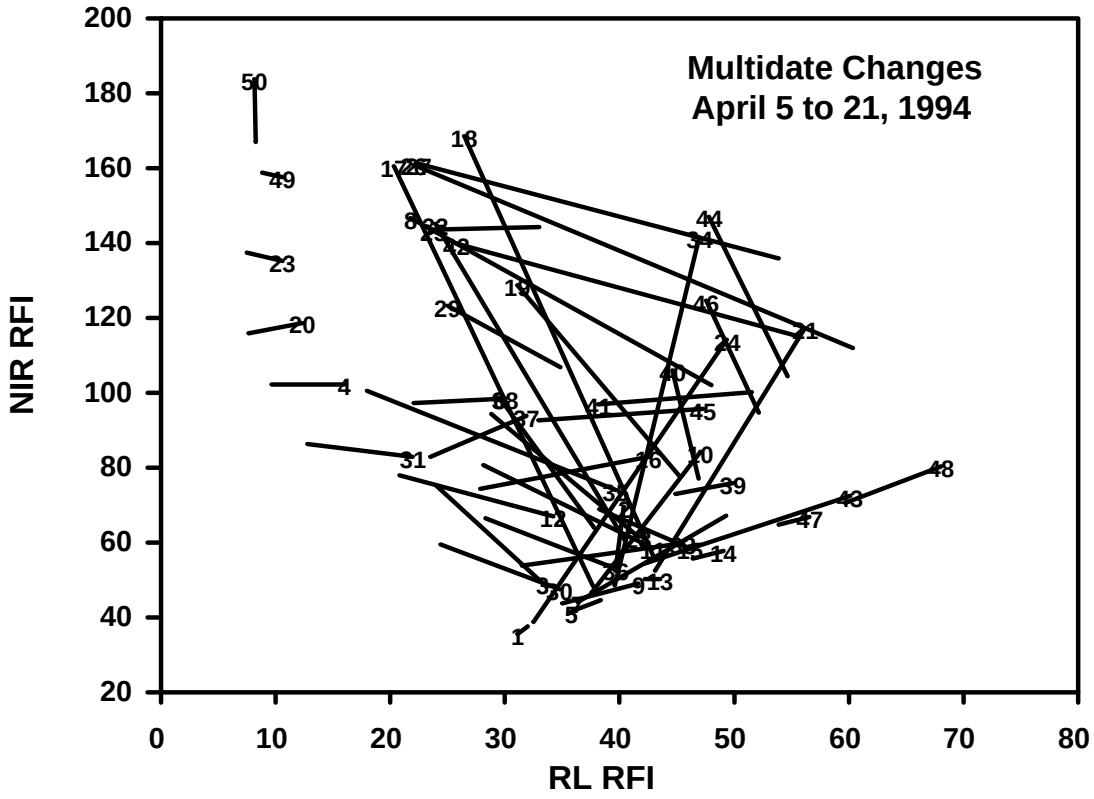

RFI here is the "reflectance factor index." RFI is equal to reflectance times 4. RFI rasters are used in a classification process to represent reflectance. The range of reflectance, R, is much less than 0 to 255. The factor of four addresses this problem.

Four RFI rasters were provided to a standard (ISODATA) clustering routine. It produced 50 classes with locations of class centers provided in NIR-RL (red light) space for both dates. Lines connect the location on April 5, 1994 with the location on April 21, 1994. The class number label is on the April 5 end of the line.

Note that the open water class (Class 1) did not change location nor spectral reflectance properties over this 16-day period of time. Green vegetation class tended to get darker in RL over the 16-day period. Class 50 (a heavily vegetated, herbaceous class on April 5) showed some decrease in NIR over the 16 day period. Classes that were beginning to yellow (probably lettuce) underwent large changes in greenness during this 16-day period of time (as lettuce harvesting was underway). Soil classes (e.g., 48, 43, 47, 14) moved up and down the Line of Bare Soils (probably due to being irrigated during the period). In general, a time sequence is seen here that starts with the Line of Bare Soils, then moves toward the 100% GC point (low RL with moderately bright NIR). Late in the season, yellowing begins and RL brightens as the NIR stays about the same (fixed leaf area index). Harvesting results in drastic changes toward yellow leaf litter or to bare soil.

Multiparameter SAR

The illustrative data set contains SAR data (SIR-C) for two wavelengths (collected simultaneously on April 15, 1994). One simple, yet effective way to view these data is by using an RGB combination (similar to what is done with optical data such as Landsat TM and SPOT XS).

When working with SAR data, the term, multispectral, does not represent all of the kinds of images possible. There are different polarization combinations as well as exotic parameters such as the absolute value of the phase different between HH and VV signals.

In general, it appears that C-band (VV) responds to leafy vegetation (herbaceous biomass) while L-band, especially cross polarization, responds to stems (woody biomass). Thus, it makes sense, in an RGB display, to assign G to C-band (VV) and to assign L-band CS to R. This leaves the B (blue) display for another raster. I used L-band VV for the other raster.

Figure 19. RGB combination of SAR image data. R = L-Band CS, G = C-Band VV & B = L-Band VV.

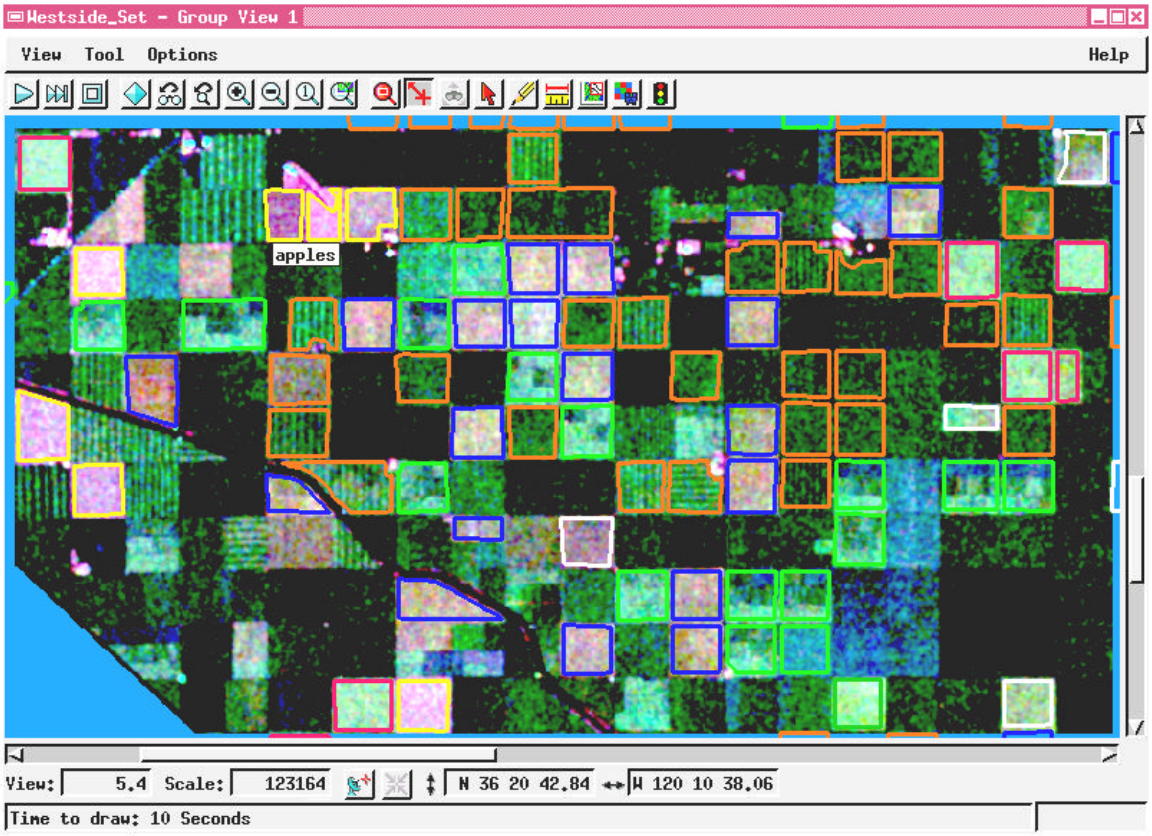

Probably the biggest difference between this SAR image and an optical MS image is the fact that woody crops (almond and apple orchards & vineyard and sugarbeets) and any crops having large, dense stalks (onions, garlic) or compact biomass (lettuce) can be detected. The varying colors suggest that the multiparameter ("color") nature of this SAR image is useful for identifying major kinds of crops in this complex scene. Many fields are bare and dry enough to be stealthy (black). Many of the tomato fields are being irrigated. These are easily seen in the C-band VV (green strips).

Multisensor Image

It is not likely that multisensor data sets will be acquired in many places in the world nor closely in time. Nevertheless, were this to be possible, each sensor has something to contribute to the mapping of scene features (Paris and Kwong, 1988; Brisco and Brown, 1995). For my example here, I have selected the GC (green cover) image from April 21, 1994 (based on NIR and RL for this date after calibration and application of the PIBA). I have put that together with an L-band image 9LAV = (LVV + LHH + 2* LCS)] and a C-Band VV image. I decided to use R for L-band, G for GC, and B for C-band VV.

Figure 20. Multisensor Combination (see text for explanation).

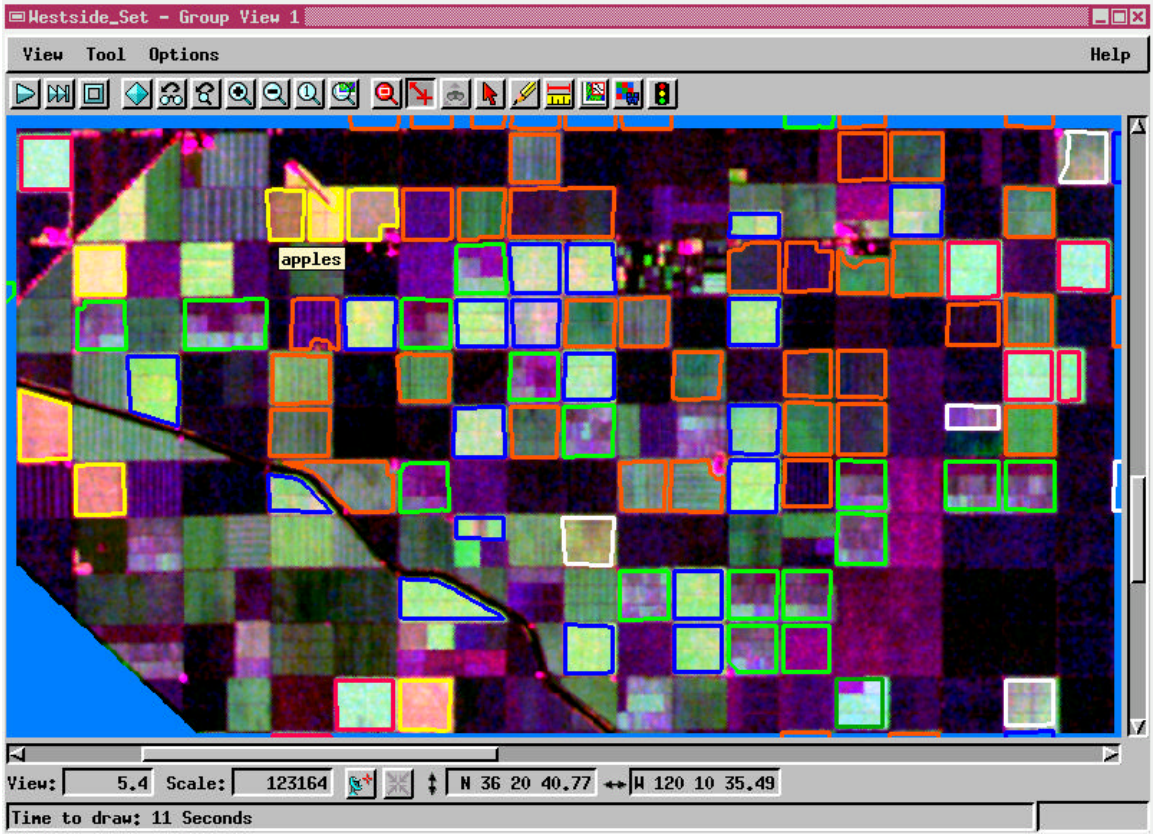

Note that most of the crop types in this region have unique RGB colors in this display combination. Sugarbeets are a light green, garlic is a similar green but with more texture, almonds are orange, apples are yellow, onions are darker than others, and emerging tomatoes are green (not bright in SAR bands yet, but detected in the GC).

The Future of Agricultural Applications of RS

Most of the foregoing discussion is based on present or experimental (not yet operational) RS capabilities. All of the examples given relate to 22-30 meter resolution data. While the spatial resolution capabilities of optical RS are better than TM, they still have a ways to go.

Over the years, I have worked with many sectors of agribusiness in attempts to serve this industry with geospatial products based on RS. Some have been successful. Others have not met the expectations of every agribusiness person. In many cases, some one has come before me with exaggerated claims about what RS will do. It has been difficult to deflate some of the high expectations regarding RS without underselling the true capabilities of RS.

Agribusiness is a tough customer for RS. It demands much. Here are some of the characteristics that would be required of an RS and its attendant geospatial technologies:

For Precision Farming:

- **Spatial Resolution.** Within field mapping of crop conditions at pixel sizes of 1-10 m are needed. End users already know what crop is growing. You can use this knowledge in approaching the RS service market. They need to know a few reliable biophysical characteristics of the known crop over subsections of the field.
- **Frequency of Coverage.** At least weekly (perhaps twice-weekly) coverage is needed. Management decisions are made once or twice weekly. RS-based information products need to be in the hands of the field managers and consultants.
- **Speed of Delivery.** Information gathered during the season needs to be provided to end-users within 24-48 hours of collection. Off-season uses are more leisurely.
- **Format for Information Products.** End users say that they only want hard copies. Certainly, hard copies are useful to take to the field. But, it is difficult to meet the speed of delivery need (and spatial resolution need) with hard copies as the only product. More and more, end users want or can deal with digital data.
- **Information Content.** End users want as much information as possible about their fields (crops and/or soils) and how these change over the season. However, they are willing to live with less than a full plate of information. For example, I have seen how effective a simple (but well calibrated) map of NDVI, provided every week or so, can be sufficient for many precision farming needs. The problem relative to information content is that a provider of information makes claims that do not hold up. It is difficult to know exactly what kind of label should be placed on a NDVI map (or even on my version – the PIBA using NIR and RL with scaling between bare soil and 100% green cover). Some have used biomass. Others present the data as being percent cover. Some mistakenly called it a vigor map or yield map. My point here is that it is much better to be conservative with respect to the label placed on an information map derived from RS data than not. Usually, the precision farmer end user just wants to know where a potential problem exists in a field and when it started. Then, he or she may investigate the “problem” area in the field using traditional approaches.

For Crop Risk Insurance:

- **Spatial Resolution.** Field to field mapping is needed. The crop risk insurance carrier needs to be able to verify that the insured crop is actually present in a field and that it is being managed in a proper manner. They need to know a few reliable biophysical characteristics of the crop over for the field as a whole. If an insured loss claim is likely due to a specific weather event, then higher resolution might be needed for that field or area.
- **Frequency of Coverage.** Insurance needs here are much less than is the case for precision farming. Some critical times of the year exist such as planting, during vegetative growth, and at harvest.

- **Speed of Delivery.** Information gathered during the season needs to be provided to end-users within 24-48 hours of collection. Off-season uses are more leisurely.
- **Format for Information Products.** End users say that they only want hard copies. Certainly, hard copies are useful to take to the field. But, it is difficult to meet the speed of delivery need (and spatial resolution need) with hard copies as the only product. More and more, end users want or can deal with digital data.
- **Information Content.** This is similar to that needed by precision farming.

Banking and Finance:

I just want to mention here an interesting application that Brazil has been doing with regard to RS and agricultural finance. INPE had a program to train loan officers in a bank to make simple, but effective interpretations of Landsat TM data in support of bank loan programs for agriculture. Basically, the bank customer was advised of the use of these data by the loan officer to inspect the development being funded.

Conclusion

The future of RS applications for agriculture is bright. Almost every RS effort today is trying to address the agribusiness market. Only a few will succeed. For example, the Resource21 effort may succeed. They plan to place 4 satellites into orbit around the earth so that the data for any given cropland area may be gathered on a weekly basis or better (for at least drier climates). Resource21 plans to use a MS RS approach with about 10-m spatial resolution with the delivery of GIS-ready information products within 24 hours of acquisition.

Just how well humid areas will be served by an approach like Resource21 is open for discussion. Other private companies will be looking towards multiparameter SAR with 1-10 m spatial resolution (at least in one band) to handle inspection needs worldwide.

Most regions will be served by aircraft-based MS systems. These can be designed with the particular needs of the service region in mind. In some cases, thermal IR approaches will work best. In other cases, MS RS will work best. In yet other cases, only radar will work. The role of hyperspectral RS in ag is not well enough understood to be a known technology.

In any case, the converging technologies of RS, GIS, GPS, YMT, VRT, etc., are in agriculture to stay.

References

Benallegue, M., O. Taconet, D. Vidal-Madjar, and N. Normand, 1995. The use of radar backscattering signals for measuring soil moisture and surface roughness. *Remote Sensing of Environment*, 53(1):61-68.

Brisco, B., and R. J. Brown, 1995. Multidate SAR/TM synergism for crop classification in western Canada. *Photogrammetric Engineering and Remote Sensing*, 61(8):1009-1114.0

Camilo, P., 1987. A canopy reflectance model based on an analytical solution to the multiple scattering equations. *Remote Sensing of Environment,* 23:453-477.

Clevers, J. G. P. W., 1988. The derivation of a simplified reflectance model for the estimation of leaf area index. *Remote Sensing of Environment*, 25:53-69.

Crippen, R. E., 1990. Calculating the vegetation index faster. *Remote Sensing of Environment*, 34:71-73.

Crist, E. P., 1985. A TM Tasselled Cap equivalent transformation for reflectance factor data. *Remote Sensing of Environment*, 17:301-306.

Davis, G., 1998. Space age farming. *Modern Agriculture*, 1(5):18-20.

Huete, A. R., 1986. Separation of soil-plant spectral mixtures by factor analysis. *Remote Sensing of Environment,* 19:237-251.

Huete, A. R., 1988. A soil-adjusted vegetation index (SAVI). *Remote Sensing of Environment,* 25:295-309.

Jackson, R. D., 1983. Spectral indices in n-space. *Remote Sensing of Environment*, 13:409-421.

Kaufman, Y. J., and D. Tanre, 1992. Atmospherically resistant vegetation index (ARVI) for EOS-MODIS, *IEEE Transactions on Geoscience and Remote Sensing,* 30(2):261-269.

Lyon, J. G., D. Yuam, R. S. Lunetta, and C. D. Elvidge, 1998. A change detection experiment using vegetation indices. *Photogrammetric Eng. & Remote Sensing.*, 64(2):143-150.

Paris, J. F., and H. H. Kwong, 1988. Characterization of vegetation with combined Thematic Mapper (TM) and Shuttle Imaging Radar (SIR-B) image data. *Photogrammetric Engineering and Remote Sensing*, 54:54:1187-1193.

Roberts, D. A., M. O. Smith, and J. B. Adams, 1993. Green vegetation, nonphotosynthetic vegetation, and soils in AVIRIS data. *Remote Sensing of Environment*, 44:253-269.

Runyon, J., 1994. Environmental management solutions for agriculture: Integrating field inspections, GIS, GPS, and aerial photography. *Geo Info Systems*, April, 42-44.

Tucker, C. J., 1979. Red and photographic infrared linear combinations for monitoring vegetation. *Remote Sensing of Environment*, 8:127-150.

Wiegand, C. L., A. J. Richardson, D. E. Escobar, and A. H. Gerbermann, 1988. Vegetation indices in crop assessments. *Remote Sensing of Environment*, 35:105-119.